Observations and modelling of the Kamchatka tsunami of 29 July 2025 for the coast of British Columbia

Alexander B. Rabinovich, Elizaveta S. Tsukanova, Richard E. Thomson, Denny C. Sinnott, and David A. Riedel

Fisheries and Oceans Canada
Institute of Ocean Sciences
9860 West Saanich Road
Sidney, BC V8L 4B2 CANADA

2026

Canadian Technical Report of Hydrography and Ocean Sciences 417

Fisheries and Oceans Canada | Pêches et Océans Canada

Canada

Canadian Technical Report of Hydrography and Ocean Sciences

Technical reports contain scientific and technical information of a type that represents a contribution to existing knowledge, but which is not normally found in the primary literature. The subject matter is generally related to programs and interests of the Oceans and Science sectors of Fisheries and Oceans Canada.

Technical reports may be cited as full publications. The correct citation appears above the abstract of each report. Each report is abstracted in the data base Aquatic Sciences and Fisheries Abstracts.

Technical reports are produced regionally but are numbered nationally. Requests for individual reports will be filled by the issuing establishment listed on the front cover and title page. Regional and headquarters establishments of Ocean Science and Surveys ceased publication of their various report series as of December 1981. A complete listing of these publications and the last number issued under each title are published in the Canadian Journal of Fisheries and Aquatic Sciences, Volume 38: Index to Publications 1981. The current series began with Report Number 1 in January 1982.

Rapport technique canadien sur l'hydrographie et les sciences océaniques

Les rapports techniques contiennent des renseignements scientifiques et techniques qui constituent une contribution aux connaissances actuelles mais que l'on ne trouve pas normalement dans les revues scientifiques. Le sujet est généralement rattaché aux programmes et intérêts des secteurs des Océans et des Sciences de Pêches et Océans Canada.

Les rapports techniques peuvent être cités comme des publications à part entière. Le titre exact figure au-dessus du résumé de chaque rapport. Les rapports techniques sont résumés dans la base de données Résumés des sciences aquatiques et halieutiques.

Les rapports techniques sont produits à l'échelon régional, mais numérotés à l'échelon national. Les demandes de rapports seront satisfaites par l'établissement auteur dont le nom figure sur la couverture et la page de titre.

Les établissements de l’ancien secteur des Sciences et Levés océaniques dans les régions et à l'administration centrale ont cessé de publier leurs diverses séries de rapports en décembre 1981. Vous trouverez dans l'index des publications du volume 38 du Journal canadien des sciences halieutiques et aquatiques, la liste de ces publications ainsi que le dernier numéro paru dans chaque catégorie. La nouvelle série a commencé avec la publication du rapport numéro 1 en janvier 1982.

Canadian Technical Report of
Hydrography and Ocean Sciences 417

2026

OBSERVATIONS AND MODELLING OF THE KAMCHATKA TSUNAMI OF 29 JULY 2025 FOR THE COAST OF BRITISH COLUMBIA

By

Alexander B. Rabinovich[1,2], Elizaveta S. Tsukanova[2],
Richard E. Thomson[1], Denny C. Sinnott[1], and David A. Riedel[1]

[1]Fisheries and Oceans Canada
Institute of Ocean Sciences
9860 West Saanich Road
Sidney, BC V8L 4B2, CANADA

[2]Shirshov Institute of Oceanology
Russian Academy of Sciences
36 Nakhimovsky Prosp.
Moscow, 117997, RUSSIA

Cat. No. Fs 97-18/417E-PDF ISBN 978-0-660-99250-1 ISSN 1488-5417

Correct citation for this publication:

Rabinovich, A.B., Tsukanova, E.S., Thomson, R.E., Sinnott, D.C., and Riedel, D.A. 2026. Observations and modelling of the Kamchatka tsunami of 29 July 2025 for the coast of British Columbia. Can. Tech. Rep. Hydrogr. Ocean Sci. 417: v + 44 p.

CONTENTS

ABSTRACT

Rabinovich, A.B., Tsukanova, E.S., Thomson, R.E., Sinnott, D.C., and Riedel, D.A. 2026. Observations and modelling of the Kamchatka tsunami of 29 July 2025 for the coast of British Columbia. Can. Tech. Rep. Hydrogr. Ocean Sci. 417: v + 44 p.

At 23:24:52 UTC on 29 July 2025, a M_w 8.8 megathrust earthquake occurred roughly 120 km seaward of Petropavlovsk-Kamchatsky off the southeastern Kamchatka Peninsula on the Pacific coast of Russia. The epicenter of the earthquake closely coincided with that of the 1952 earthquake, which generated a highly catastrophic tsunami that killed about 15,000 people on the coasts of the North Kuril Islands and the southern Kamchatka Peninsula. In contrast, the 2025 tsunami caused minimal damage and no fatalities. As with the 1952 event, waves from the 2025 earthquake spread throughout the Pacific Ocean and markedly affected the coasts of the Hawaiian Islands, California, British Columbia and Chile. The tsunami was observed along the entire coast of British Columbia (BC), where it was recorded by 26 Canadian Hydrographic Service (CHS) tide gauges. The first wave arrived at Henslung Cove 6 h 24 min after the main shock and then, about 1.0-1.5 hours later, at the mainland coast of BC (Prince Rupert, Pruth Bay and Bella Bella) and on the outer coast of central and southern Vancouver Island (Tofino, Ucluelet, Bamfield and Port Renfrew). The maximum observed tsunami wave height of 94 cm was recorded at Port Alberni on southern Vancouver Island; 54 cm waves were observed at Winter Harbour on northwestern Vancouver Island. Typical wave periods ranged from 20 to 110 min. Waves from the 2025 tsunami were recorded at 11 deep-water Ocean Networks Canada (ONC) sites and at DART 46419 located offshore of Vancouver Island. Maximum amplitudes increased from 4.7 4.9 cm at 9 deep stations (depth 2193-2815 m) to 13.3 cm at the shallowest site, Folger Passage station (depth 95 m). The first wave arrived at the DART and ONC stations 60-70 min earlier than at the nearby coast of Vancouver Island, indicating that these stations can be used effectively for the early tsunami warning. Comparison of the 1952 and 2025 events indicates that the mean ratio (1952/2025) of the recorded heights was ~1.60. Our numerical simulation of the 2025 tsunami yielded computed waveforms that are in near perfect agreement with the recorded tsunami waveforms for the offshore stations; comparisons for coastal stations reveal that improved spatial model resolution and nested grids are needed.

RÉSUMÉ

Rabinovich, A.B., Tsukanova, E.S., Thomson, R.E., Sinnott, D.C., and Riedel, D.A. 2026. Observations and modelling of the Kamchatka tsunami of 29 July 2025 for the coast of British Columbia. Can. Tech. Rep. Hydrogr. Ocean Sci. 417: v + 44 p.

Le 29 juillet 2025 à 23h24min52 UTC, un séisme de magnitude 8,8 s'est produit à environ 120 km au large de Petropavlovsk-Kamtchatski, au sud-est de la péninsule du Kamtchatka, sur la côte Pacifique de la Russie. L'épicentre de ce séisme coïncidait presque avec celui du séisme de 1952, qui avait engendré un tsunami dévastateur ayant fait environ 15 000 victimes sur les côtes des îles Kouriles du Nord et du sud de la péninsule du Kamtchatka. À l'inverse, le tsunami de 2025 n'a causé que des dégâts minimes et aucune victime. Comme en 1952, les vagues du séisme de 2025 se sont propagées dans tout l'océan Pacifique et ont fortement affecté les côtes des îles Hawaïennes, de la Californie, de la Colombie-Britannique et du Chili. Le tsunami a été observé sur toute la côte de la Colombie-Britannique, où il a été enregistré par 26 marégraphes du Service hydrographique du Canada. La première vague est arrivée à Henslung Cove 6 h 24 min après le choc principal, puis, environ 1,0 à 1,5 heure plus tard, sur la côte continentale de la Colombie-Britannique (Prince Rupert, Pruth Bay et Bella Bella) et sur la côte extérieure du centre et du sud de l'île de Vancouver (Tofino, Ucluelet, Bamfield et Port Renfrew). La hauteur maximale des vagues du tsunami observée, soit 94 cm, a été enregistrée à Port Alberni, au sud de l'île de Vancouver ; des vagues de 54 cm ont été observées à Winter Harbour, au nord-ouest de l'île de Vancouver. Les périodes typiques des vagues variaient de 20 à 110 minutes. Les vagues du tsunami de 2025 ont été enregistrées à 11 stations en eaux profondes du réseau Ocean Networks Canada (ONC) et à la station DART 46419, située au large de l'île de Vancouver. Les amplitudes maximales sont passées de 4,7 à 4,9 cm à 9 stations profondes (profondeur de 2 193 à 2 815 m) à 13,3 cm à la station la moins profonde, Folger Passage (profondeur de 95 m). La première vague est arrivée aux stations DART et ONC 60 à 70 minutes plus tôt qu'à proximité de la côte de l'île de Vancouver, ce qui indique que ces stations peuvent être utilisées efficacement pour l'alerte précoce aux tsunamis. La comparaison des événements de 1952 et de 2025 indique que le rapport moyen (1952/2025) des hauteurs enregistrées était d'environ 1,60. Notre simulation numérique du tsunami de 2025 a produit des formes d'onde calculées qui correspondent presque parfaitement aux formes d'onde enregistrées par les stations au large ; les comparaisons pour les stations côtières révèlent qu'une meilleure résolution spatiale du modèle et des grilles emboîtées sont nécessaires.

The Pacific coast of the Kamchatka Peninsula [from russiadiscovery.ru]

1. INTRODUCTION

At 23:24:52 UTC on 29 July 2025, a M_w 8.8 megathrust earthquake occurred seaward of the southeastern Kamchatka Peninsula on the Pacific coast of Russia. According to the United States Geological Survey (USGS), the epicenter of the earthquake was located at 52.473° N, 160.396° E, about 120 km southeast from Petropavlovsk-Kamchatsky, the capital of the Kamchatka Krai, at a hypocenter depth of ~35 km. The earthquake was the sixth strongest ever instrumentally recorded, tied with the 2010 Chile (M_w 8.8) earthquake and weaker than only the 1960 Chile (9.5), 1964 Alaska (9.2), 2004 Sumatra (9.1-9.3), 2011 Tohoku (9.1) and 1952 Kamchatka (9.0) earthquakes. The source area of the 2025 earthquake coincided closely with that of the 1952 earthquake that generated a highly catastrophic tsunami, which obliterated the town of Severo-Kurilsk (Paramushir Island) and several small villages along the coasts of the North Kuril Islands and southern Kamchatka. Roughly 15,000 people were killed at these locations [*Shevchenko et al.*, 2022; *Gusiakov,* 2025]. The tragic 1952 event led to the initiation of the Russian Tsunami Warning Service. In contrast, the 2025 tsunami caused minimal damage and no fatalities. The marked dissimilarity between the two events gave rise to several puzzling questions [*Miller*, 2025; *Andrews*, 2025; *Steedman*, 2005]: “Why did such a powerful earthquake generate such a weak tsunami?” and “Why was the damage so minimal?”. Our

study demonstrates that the 2025 tsunami was not weak and that the waves spread throughout the entire Pacific Ocean and affected the coasts of the Hawaiian Islands, California and Chile. Remarkably, the waves also went through the Drake Passage and penetrated into the Atlantic Ocean. In the near-field area of the southeastern Kamchatka Peninusla, tsunami runup was as high as 18 m. In the area of the old town of Severo-Kurilsk (totally destroyed by the 1952 tsunami), the observed tsunami heights were up to 9 m.

The 2025 Kamchatka tsunami waves were clearly recorded by multiple tide gauges along the coast of British Columbia. The purpose of this report is to estimate statistical parameters of the measured waves, present waveforms from numerical simulations of the two tsunamis, and to compare the 1952 and 2025 events as they were observed along the BC coast.

2. OBSERVATIONS

Observations from the Pacific Tsunami Warning Center (PTWC) and the National Tsunami Warning Center (NTWC) show that the Kamchatka tsunami of 29 July 2025 spread over the entire Pacific Ocean and was recorded along the coast of North America, including by the Canadian Tsunami Warning Stations (Henslung, Winter Harbour, Tofino and Port Alberni). To study this event, we selected records from 27 tide gauge stations. Information regarding the instruments is presented in Table 1; tide gauge locations are shown in Figure 2. In all tide gauge records, except Sand Heads, the tsunami signal is clearly identified. It appears that the reason why the tsunami was not detected at Sand Heads record is that the tsunami amplitudes at this station were too small and had a too low signal-to-noise (s/n) ratio.

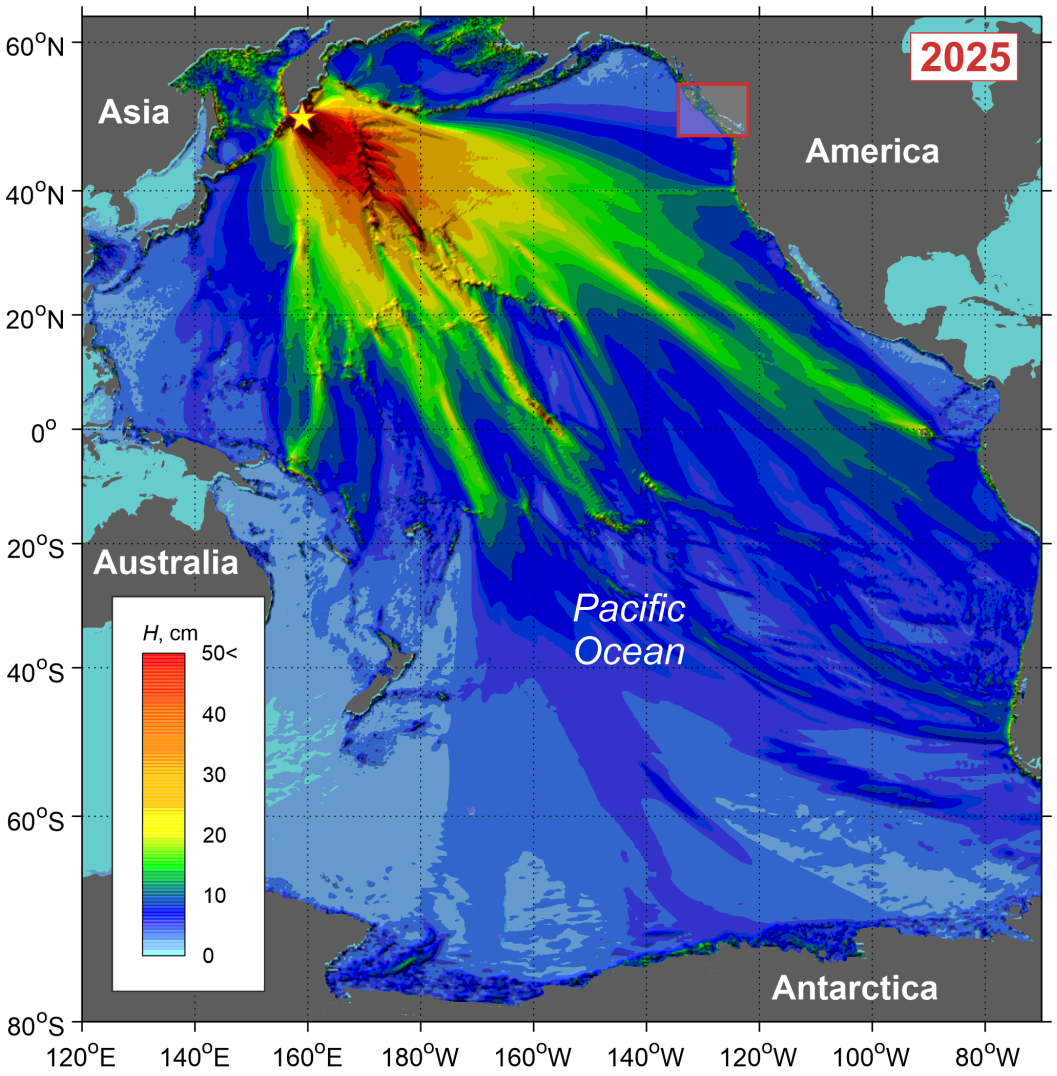

Figure 1. Numerically simulated maximum wave amplitudes of the 2025 Kamchatka tsunami for the Pacific Ocean. The yellow star indicates the epicenter of the earthquake (M_w 8.8); the red box frames the area of British Columbia.

For practical purposes, we separated the stations into four geographical groups: (1) the *Southwestern* (SW) group that includes eight stations located along the oceanic coast of Vancouver Island, plus Victoria and Sidney (Figure 2a); (2) the *Southeastern* (SE) group of four stations located in Saanich Inlet and the Strait of Georgia (Figures 2c and 2d); (3) the *North-Central* (NC) group, including two stations on the southern coast of Dixon Entrance and four stations in the area of Queen Charlotte Sound (Figure 2a); and (4) the *Northeastern* (NE) group of eight stations containing five stations in the area of Prince Rupert, two stations – Hartley Bay and Kitimat – in Douglas Channel, and the Daajing Giids station (former Queen Charlotte City) on the inner side of Haida Gwaii (Figures 2a and 2b).

Table 1. Boilerplate information for the CHS tide gauges positioned along the coast of British Columbia that were used to examine the 2025 Kamchatka tsunami. (See Figure 1 for locations.)

Station	Coordinates		Region	Type	Instrument *	Established	Present deployment
	Latitude (°N)	Longitude (°W)					
Prince Rupert	54.3170	130.3240	Northern BC	Permanent	SW	1906	1909-01-01
Prince Rupert RoRo	54.2349	130.3351	Northern BC	Permanent	R	2018	2018-05-31
Fairview Terminal	54.2903	130.3599	Northern BC	Permanent	R	2014	2014-10-09
Pembina Terminal	54.2363	130.3035	Northern BC	Permanent	R	2021	2021-01-19
Porpoise Channel	54.2152	130.2891	Northern BC	Permanent	R	2013	2013-09-11
Kitimat	53.9890	128.6960	Central BC	Permanent	R	1951	2012-03-18
Hartley Bay	53.4242	129.2519	Central BC	Permanent	PB	1909	2016-03-15
Henslung Cove	54.1910	133.0020	Langara I.	Permanent	PB	1983	2006-03-18
Masset	54.0100	132.1410	NE Graham I.	Permanent	R	2008	2008-06-20
Daajing Giids (QCC)	53.2520	132.0720	SE Graham I.	Permanent	SW	1957	1963-06-01
Rose Harbour	52.1552	131.0909	N Kunghit I.	Permanent	PB	1935	2014-03-24
Bella Bella	52.1630	128.1430	Central BC	Permanent	SW	1961	1961-07-15
Pruth Bay	51.6545	128.1295	Central BC	Temporary	R	2018	2018-05-31
Port Hardy	50.7220	127.4890	NE Vancouver I.	Permanent	SW	1964	1964-06-04
Winter Harbour	50.5130	128.0290	NW Vancouver I.	Permanent	SW	1963	1989-02-01
Tofino	49.1540	125.9130	W Vancouver I.	Permanent	SW	1905	1905-08-30
Ucluelet	48.9470	125.5520	W Vancouver I.	Permanent	R	2019	2019-03-28
Port Alberni	49.2256	124.8136	C Vancouver I.	Permanent	SW	1970	1970-12-01
Bamfield	48.8360	125.1360	S Vancouver I.	Permanent	SW	1969	1969-10-01
Port Renfrew	48.5550	124.4210	S Vancouver I.	Permanent	R	1968	1968-02-01
Victoria	48.4247	123.3707	S Vancouver I.	Permanent	SW	1905	1895-02-01
Sidney	48.6492	123.3929	S Vancouver I.	Permanent	R	1992	2011-08-31
Patricia Bay	48.6536	123.4515	S Vancouver I.	Permanent	SW	1976	1976-06-04
Bamberton	48.5887	123.5214	S Vancouver I.	Temporary	PB	2021	2021-11-10
Sand Heads	49.1052	123.3042	Southern BC, SoG	Permanent	R	2002	2002-06-04
Point Atkinson	49.3375	123.2536	Southern BC, SoG	Permanent	SW	1897	1914-05-01
Nanaimo	49.1628	123.9235	E Vancouver I.	Permanent	R	1997	1997-01-01

* PB = pneumatic bubbler; SW = optical encoder/stilling well; R = open air radar. NE = Northeastern, SE = Southeastern, N = Northern, NW = Northwestern, W = Western, S = Southern, E = Eastern, C = Central, and SoG=Strait of Georgia.

Figure 2. (a) Map of British Columbia (BC) showing locations of the Canadian Hydrographic Service (CHS) coastal tide gauges (TGs) that are used in the present study; the TGs are divided into four groups: Northeastern (NE), North-Central (NC), Southeastern (SE) and Southwestern (SW); DG = Daajing Giids, *DC* = Douglas Channel, *AI* = Alberni Inlet; (b) The area of Prince Rupert with locations of five stations of the NE group; three more NE stations – Daajing Giids (DG), Kitimat and Hartley Bay – are displayed in (a); (c) Southeastern part of BC showing locations of all four stations of SE group, two stations (Victoria and Sidney) of the SW group and station Sand Heads, where no tsunami signal was identified; and (d) The area of the Saanich Peninsula and Saanich Inlet showing the locations of stations Sidney, Patricia Bay and Bamberton. Because the Sand Heads station (white circle) did not record the tsunami, the tide gauge signal was not plotted or analyzed.

All of the tide gauges listed above are from the Canadian Hydrographic Service (CHS). Destructive tsunamis in the 1990s in the Pacific Ocean initiated CHS in 1997 to provide a major upgrade of the existing network of tide gauges on the BC coast, including those located in Dixon Entrance and Queen Charlotte Sound [*Rabinovich and Stephenson*, 2004; *Stephenson and Rabinovich*, 2009]. Several more permanent and temporary instruments were deployed recently (including a group of stations in the Prince Rupert area and at Bamberton in Saanich Inlet).

The digital records from all coastal stations were examined using the data analysis procedures and tsunami detection methods described by *Rabinovich et al.* [2006, 2013, 2017]. Specifically, we verified and corrected all data, subtracted predicted tides from the original records and high-pass filtered the de-tided time series using a 4-h Kaiser-Bessel (KB) window [cf. *Thomson and Emery* 2024] to suppress low-frequency sea level fluctuations, mainly associated with atmospheric processes. These filtered sea level time series were then used to construct plots of tsunami records (Figures 3-4) for various sites and to estimate statistical characteristics of the recorded tsunami waves (Table 2). The 2025 Kamchatka tsunami waves were identified in all records except Sand Heads.

3. RESULTS: TIDE GAUGE DATA

Statistical characteristics of the 2025 Kamchatka tsunami waves on the coast of British Columbia are presented in Table 2; residual (de-tided) and high-pass filtered (with a 4-hour KB window) sea level time series are shown in Figures 3 (for 3-day segments) and 4 (for 1.25-day segments). The tsunami waves approaching the BC coast first arrived at Henslung Cove, Langara Island (the northernmost station of the CHS water level network used in this study; see Figure 2a) on 30 July at 05:49 UTC, i.e., 6 h and 24 min after the main earthquake shock. A northern branch of the tsunami wave field went through Dixon Entrance and reached Masset at 06:39 UTC. At 06:57-07:05 UTC (7h and 32-40 min after the earthquake), the waves reached the group of five CHS stations in the Prince Rupert area (Figure 2b, Table 2). The main tsunami energy went in the direction of Haida Gwaii and Vancouver Island; at 06:06 UTC the waves arrived at Rose Harbour (southern Haida Gwaii), then, subsequently, at Winter Harbour (06:35 UTC), Tofino (07:08), Ucluelet (07:17), Bamfield (07:20), Port Renfrew (07:27) and Victoria (08:08). The tsunami waves that went through Juan de Fuca Strait entered the southern Strait of Georgia and were measured at Sidney (08:38), Point Atkinson (08:54) and Nanaimo (09:39). A minor branch of the tsunami wave radiation turned the corner around the Saanich Peninsula

(Figure 2d) and penetrated into Saanich Inlet, where it was recorded at Patricia Bay (09:02) and Bamberton (09:12).

The tsunami waves from the 2025 event that propagated through Queen Charlotte Sound arrived at the mainland coast of central British Columbia and were measured at Pruth Bay (06:55 UTC) and Bella Bella (07:09 UTC). After propagating northward within Hecate Strait, the waves entered Douglas Channel and were subsequently observed at Hartley Bay (07:18) and even at Kitimat (07:40), located at the head of Kitimat Arm, the distant continuation of Douglas Channel. The arrival times at all stations were consistent and in good agreement with the theoretical (kinematically computed) arrival times (Expected Time of tsunami Arrival, ETA). In general, the 2025 Kamchatka event was the second tsunami in the 21st century that was intensively instrumentally recorded at 26 stations along the coast of British Columbia, second only to the 2022 Tonga volcanic tsunami recorded at 32 stations and ahead of the 2011 Tohoku tsunami recorded at 20 stations.

The maximum tsunami trough-to-crest wave heights of 94 cm and amplitude of 51 cm were recorded at Port Alberni (Table 2, Figures 3a and 4a). Tsunami waves at this station, located at the head of the very long and narrow Alberni Inlet, arrived at 07:47 UTC on 30 July 2025, about 27-30 min later then the waves that arrived at Ucluelet and Bamfield, two stations located on the oceanic coast of Vancouver Island, close to the entrance to Alberni Inlet (Figure 2a). The second highest waves of 54 cm wave height and 24 cm amplitude were recorded at Winter Harbour, on the northwestern coast of Vancouver Island. At three more stations, Tofino, Ucluelet (both on the oceanic coast of Vancouver Island) and Henslung Cove (Langara Island, Dixon Entrance), the recorded wave heights were about 40-45 cm. At other stations, the recorded heights were smaller: 30-34 cm at Bamfield and Port Renfrew (Figure 3a and 4a), 21-29 cm at Rose Harbour, Pruth Bay and Bella Bella (Figures 3c and 4c), 24 cm at Victoria and 13 cm at Sidney (Figures 3a and 4a). For the entire North-Central group, including five stations around Prince Rupert, Daajing Giids, Hartley Bay and Kitimat, tsunami waveforms were mutually consistent, despite their relatively small heights of 5.5-16 cm (Figures 3d and 4d). The smallest, but still detectable waves of 3.4-6 cm, were observed for the highly sheltered Southeastern group of stations located in the southern Strait of Georgia and in Saanich Inlet (Figures 3b and 4b). The only exception is Sand Heads; no tsunami waves were detected at this station, so the sea level records are not shown.

The first wave was positive at all stations, reaching maximum recorded amplitudes at Port Alberni (30.6 cm) and Winter Harbour (20.9 cm). At no station was the highest wave associated with the first wave, but were recorded several hours later. For example, at Winter

Harbour the highest wave amplitude of 23.9 cm was observed at 21:04 UTC, roughly 14 hours after the first arrival of tsunami waves at this station, while at most of the stations of the Prince Rupert group, the maximum waves were measured after midnight, 15-18 hours after the first wave arrivals (Table 2). The long (3-4 day) ringing and complicated structure of the recorded waves along the BC coast appear to be related to multiple reflection of propagating waves from various bathymetric and coastal features and to multi-ray arrivals.

Table 2. Parameters of the Kamchatka tsunami of 29 July 2025 recorded on the coast of British Columbia. All arrival times and times of the maximum waves (in UTC hours) are for 30 July 2025, except those indicated by *. (Earthquake M_w 8.8 at 23:25 UTC on 29 July 2025).

Station	First wave			Max waves			Period$^+$ (min)
	Arrival time (UTC)	Travel time (hh:mm)	Ampli-tude (cm)	Max ampli-tude (cm)	Time (UTC) of max amplitude	Max wave height (cm)	
Prince Rupert	06:58	07:33	+3.1	8.0	02:05*	16.0	110
Prince Rupert RoRo	06:57	07:32	+2.1	4.5	22:32	9.1	110, 27
Fairview Terminal	06:59	07:34	+2.9	6.8	00:29*	13.5	110
Pembina Terminal	06:57	07:32	+3.6	5.3	01:30*	12.1	110, 48
Porpoise Channel	07:05	07:40	+3.0	4.3	01:31*	10.3	110, 50
Kitimat	07:40	08:15	+4.0	4.9	22:52	8.7	105-120, 28
Hartley Bay	07:18	07:53	+2.9	3.1	09.57	5.5	70, 46, 20
Henslung Cove	05:49	06:24	+8.6	17.4	11:45	39.4	25, 12
Masset	06:39	07:14	+3.7	8.8	21:58	20.0	65
Daajing Giids (QCC)	08:27	09:02	+1.8	5.1	13:20	10.7	40,32,14,8
Rose Harbour	06:06	06:41	+8.9	15.1	14:59	29.0	20, 43, 5
Bella Bella	07:09	07:44	+7.2	9.7	09:08	20.8	43, 80, 10
Pruth Bay	06:55	07:30	+6.9	12.0	08:43	25.6	24, 80, 10
Port Hardy	07:20	07:55	+6.8	7.9	14:00	18.3	10,24,7,70
Winter Harbour	06:35	07:10	+20.9	23.9	21:04	54.0	23, 48, 67
Tofino	07:08	07:43	+15.6	21.8	11:33	44.5	19, 75
Ucluelet	07:17	07:52	+13.0	21.6	11:36	41.9	22, 86
Port Alberni	07:47	08:22	+30.6	51.0	00:20*	94.0	80-110
Bamfield	07:20	07:55	+11.5	13.6	09:21	29.7	18,27,70,4
Port Renfrew	07:27	08:02	+11.1	17.0	09:47	33.6	33, 6
Victoria	08:08	08:43	+6.0	12.6	11:48	24.0	23, 67

Sidney	08:38	09:13	+3.8	7.4	13:02	13.1	30, 60
Patricia Bay	09:02	09:37	+2.0	3.1	22:06	5.8	26, 9
Bamberton	09:12	09:47	+2.0	3.3	14:11	6.0	32, 12
Point Atkinson	08:54	09:29	+1.9	2.1	00:40*	3.4	33, 75
Nanaimo	09:39	10:14	+0.6	1.9	17:52	4.1	23

* 31 July 2025;

[+] Periods are given in order of importance.

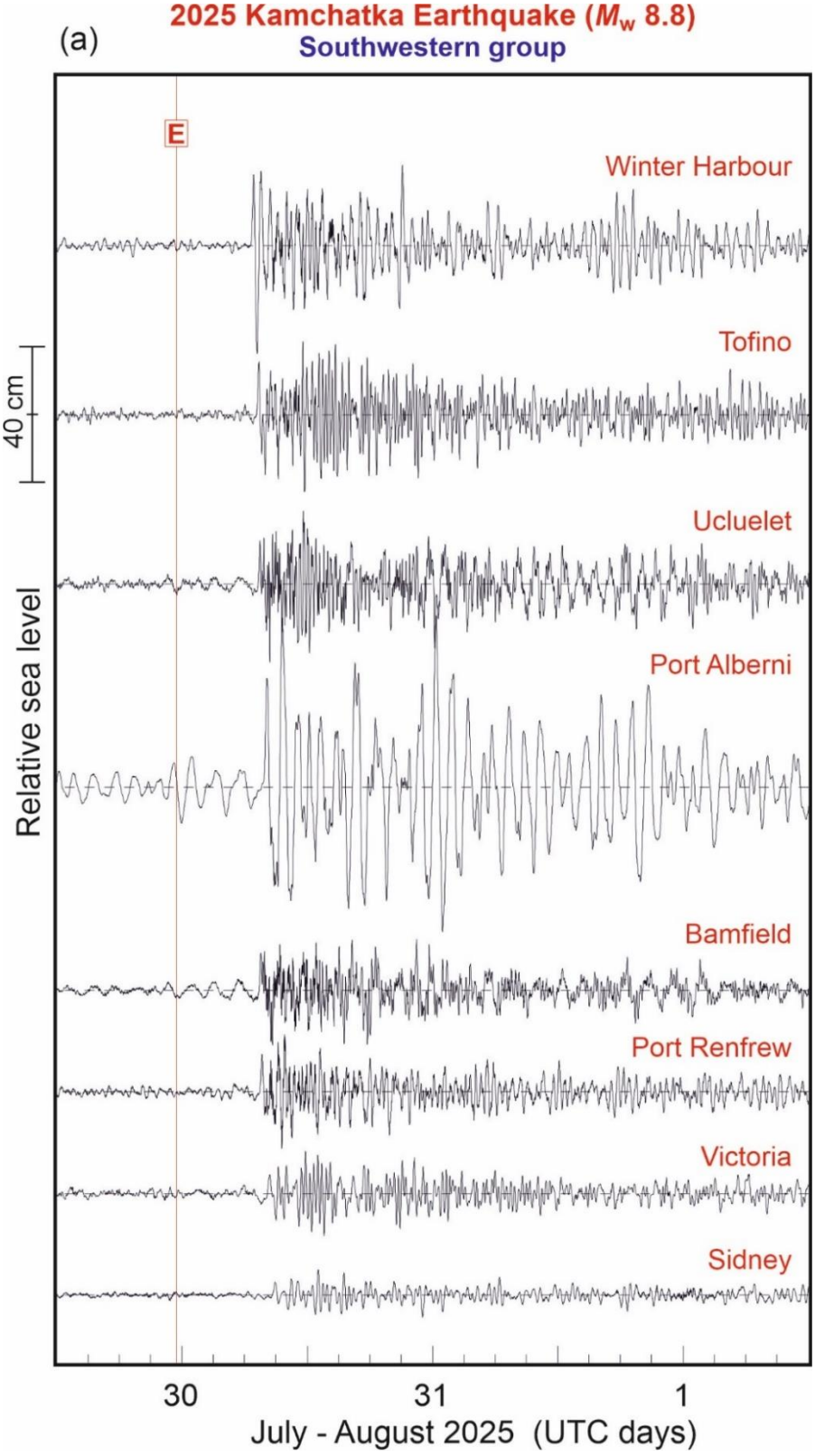

Figure 3. De-tided and high-pass filtered (4-hour Kaiser-Bessel window) 3-day records of the 2025 Kamchatka tsunami at the Canadian Hydrographic Service (CHS) tide gauges located along the coast of British Columbia. The solid vertical red line labelled "E" indicates the time of the earthquake. The individual records are shifted in the vertical relative to each other. (a) Southwestern group of stations.

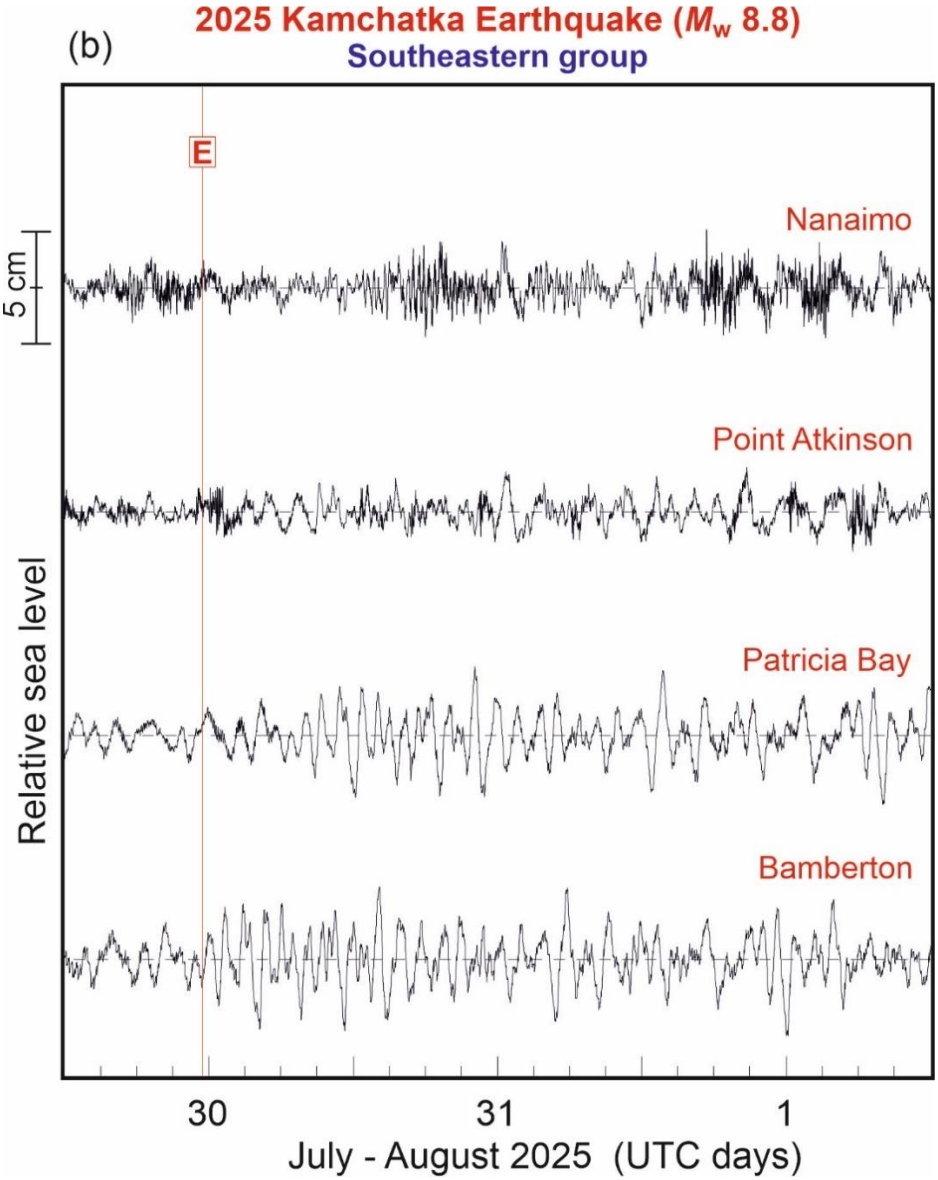

Figure 3. Continuation. (b) Southeastern group of stations.

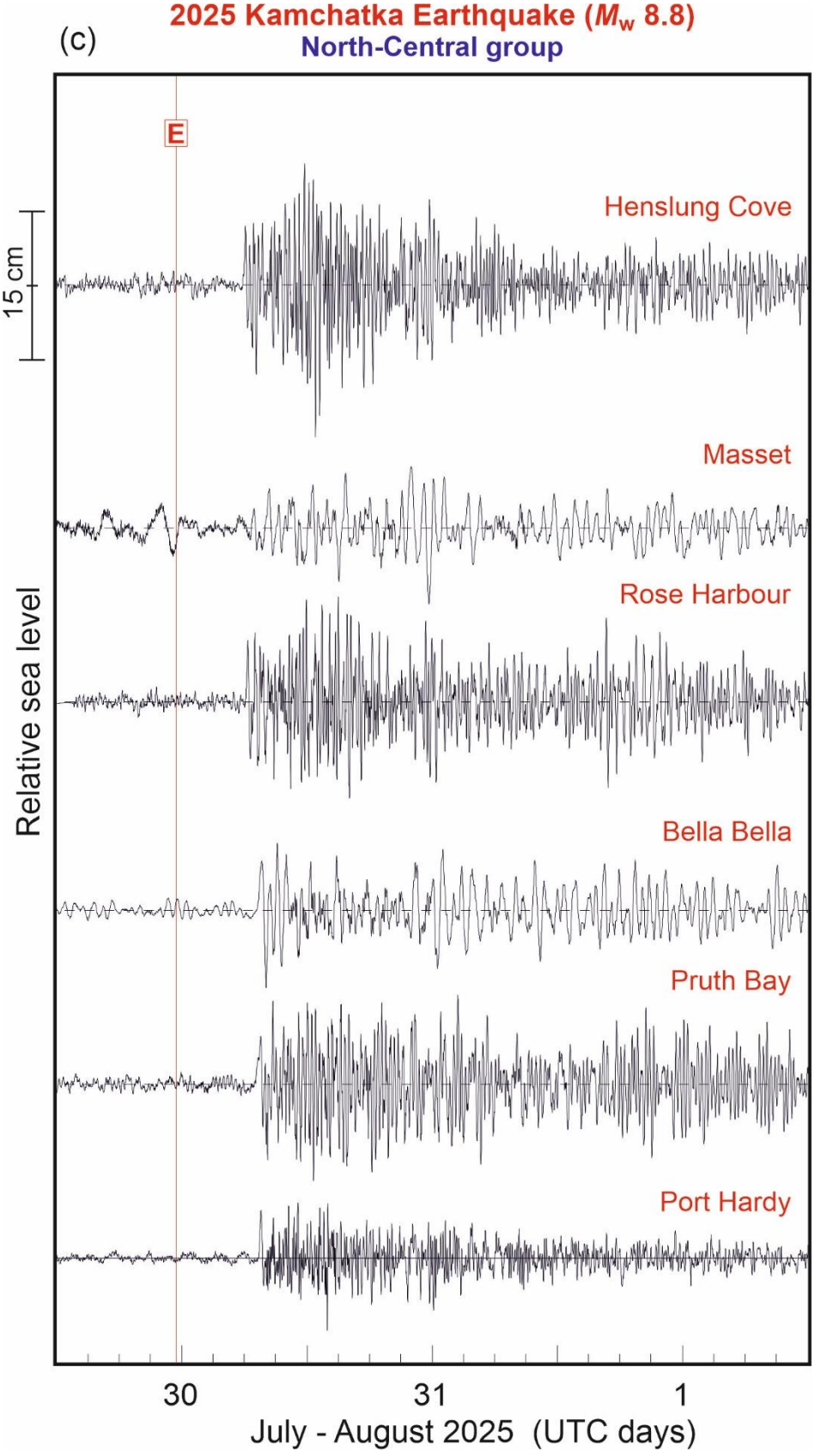

Figure 3. Continuation. (c) North-Central group of stations.

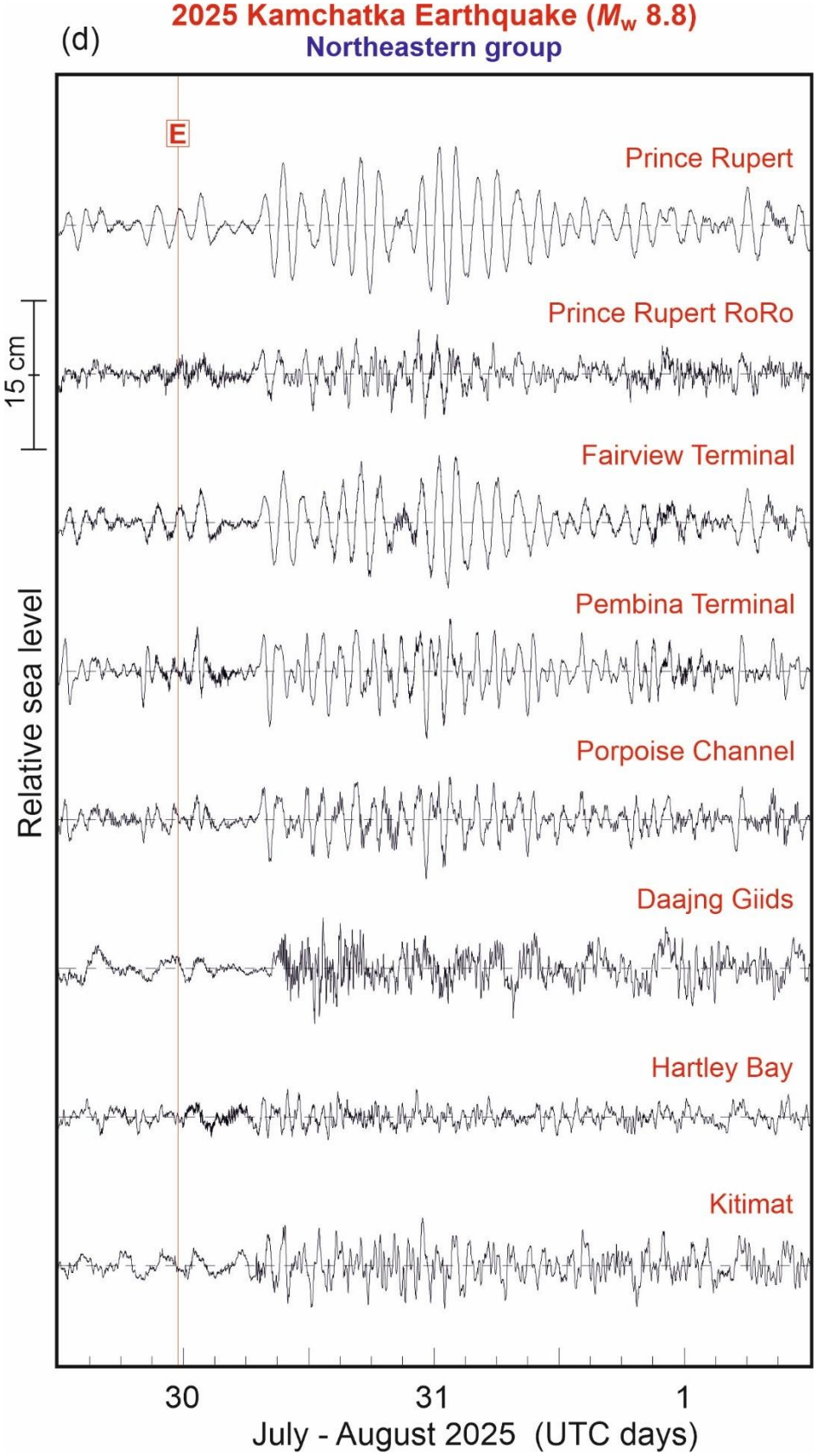

Figure 3. Continuation. (d) Northeastern group of stations.

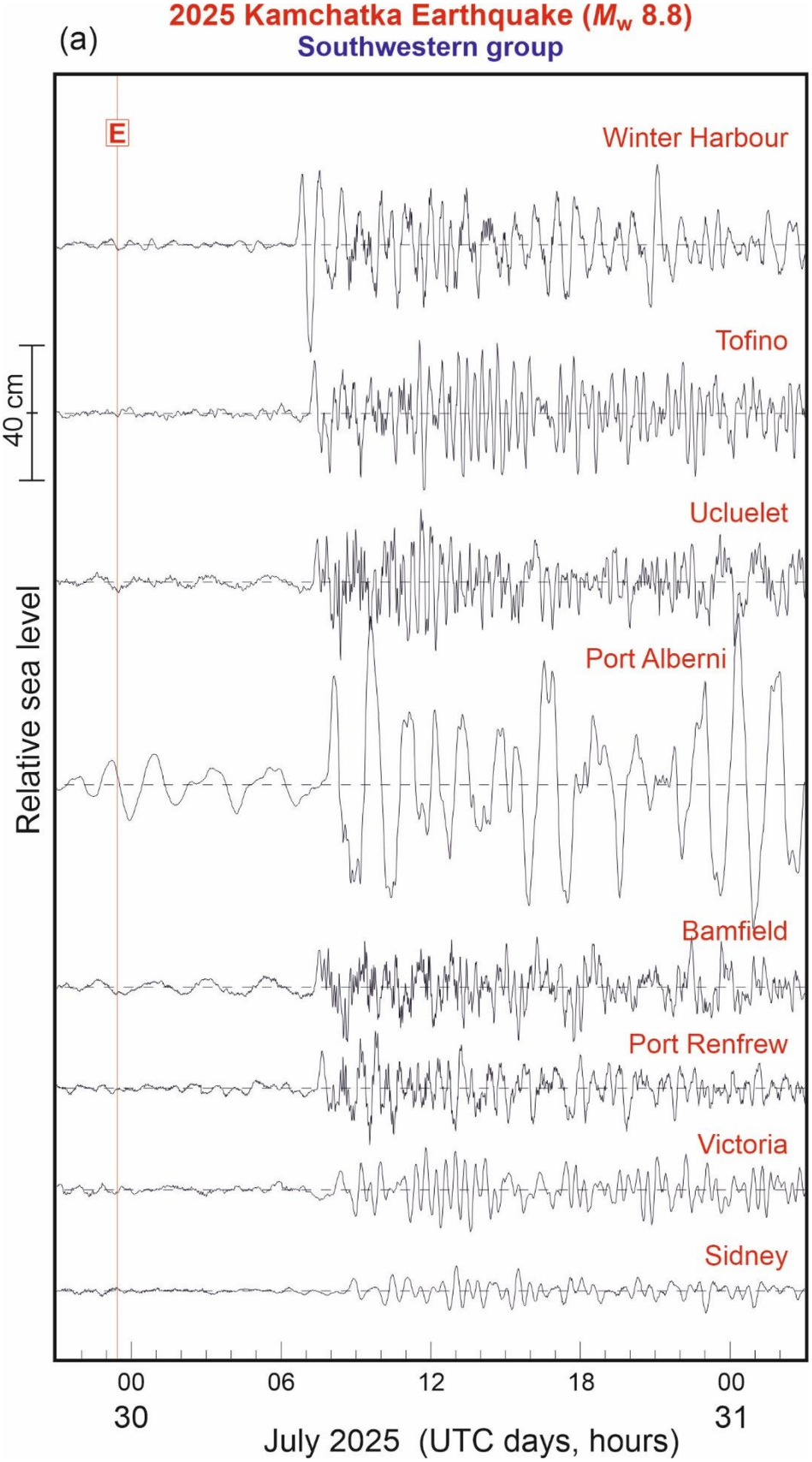

Figure 4. The same as in Figure 3 but for 1.25-day segments. (a) Southwestern group of stations.

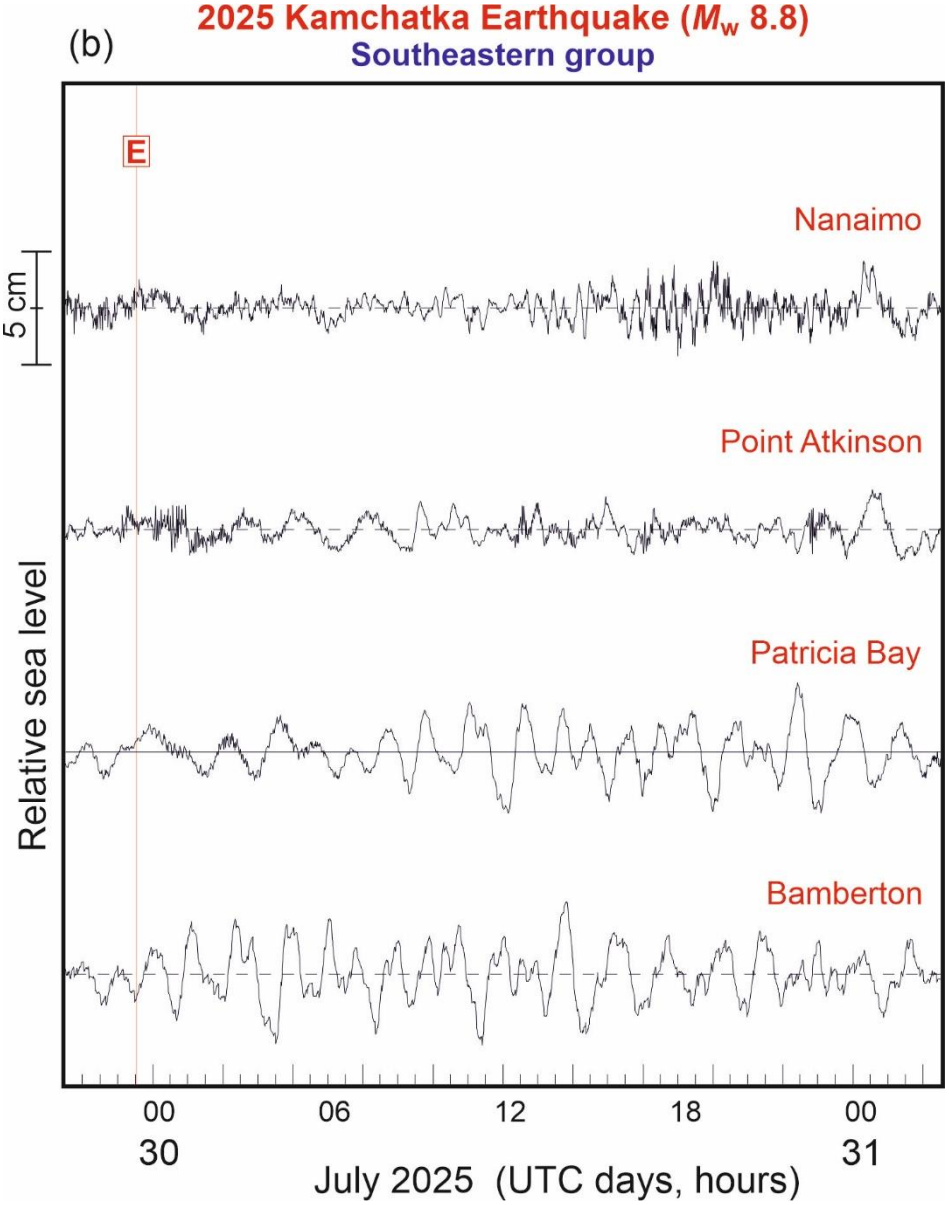

Figure 4. Continuation. (b) Southeastern group of stations.

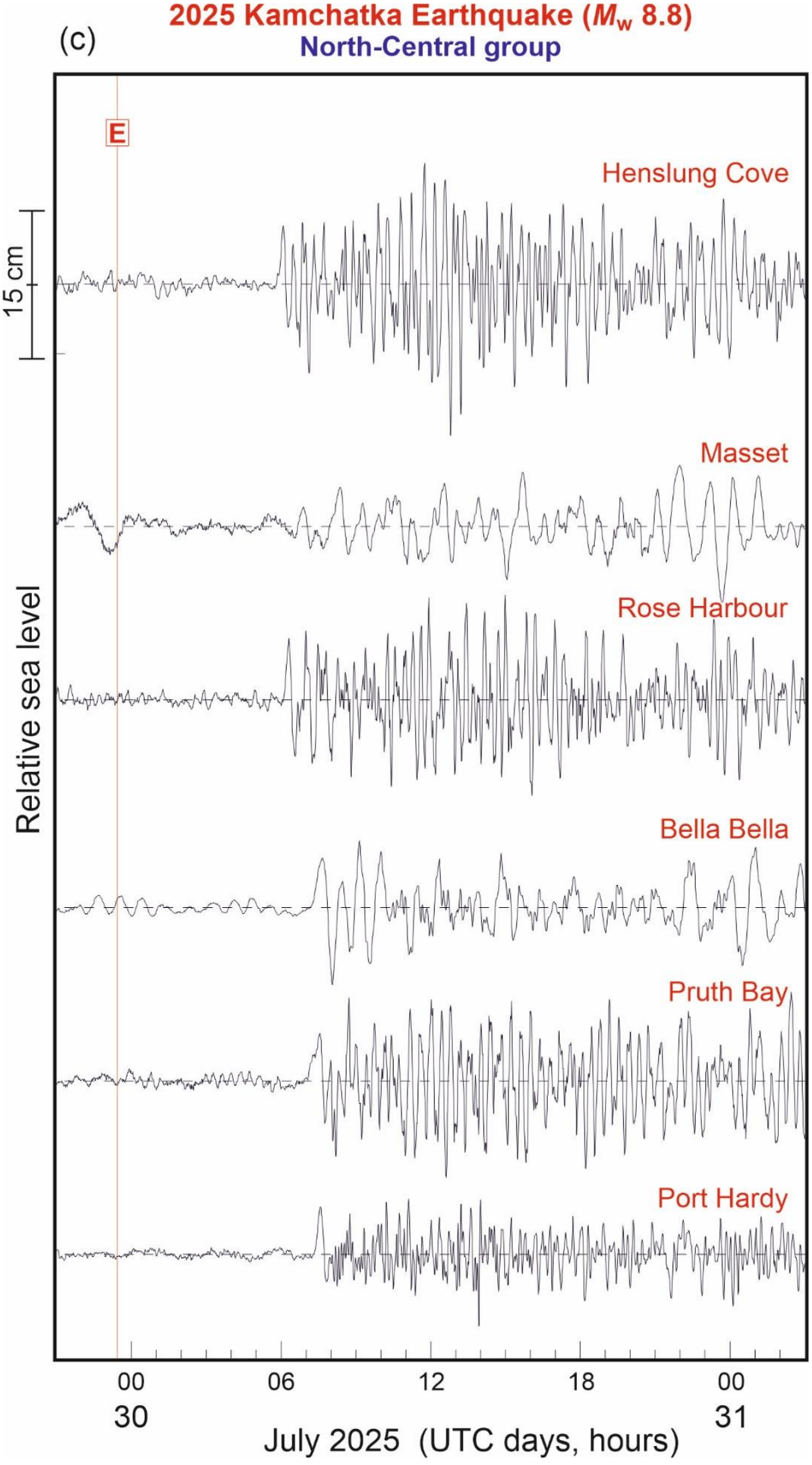

Figure 4. Continuation. (c) North-Central group of stations.

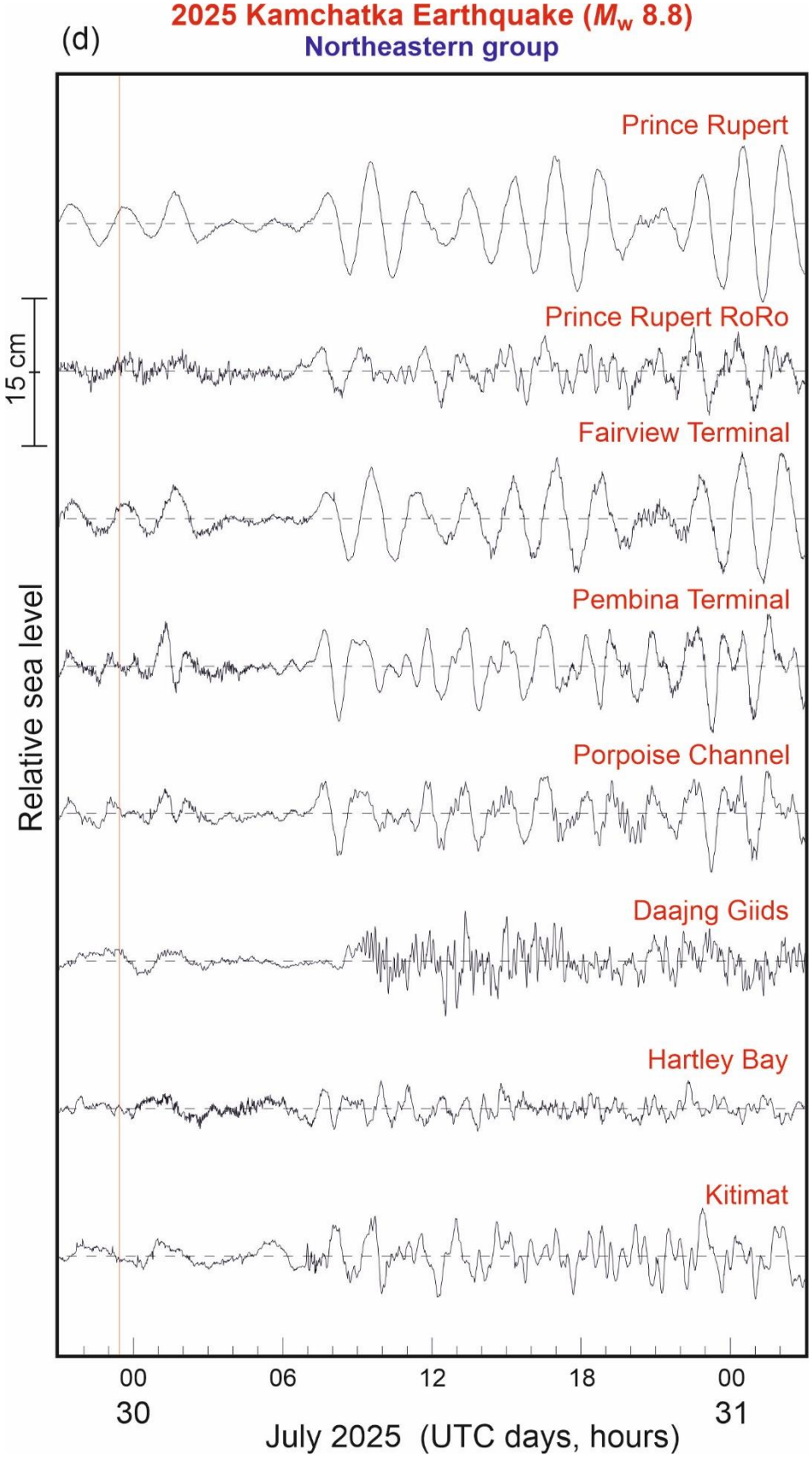

Figure 4. Continuation. (d) Northeastern group of stations.

To examine temporal variations of high-frequency sea level fluctuations in the frequency domain and to estimate the dominant periods of recorded tsunami oscillations at the various British Columbia coastal sites, a multiple-filter method, similar to wavelet analysis was used [cf. *Thomson and Emery*, 2024]. This method has been effectively applied previously to investigate various tsunami events [cf. *Rabinovich et al.*, 2006, 2013, 2017, 2019; *Zaytsev et al.*, 2017]. It enables the investigator to determine changes in propagating waves as a function of frequency, f, and time, t, and to build so called $f-t$ diagrams that display possible nonstationary properties of the waves. The *f-t* diagrams for stations from the Southwestern (SW), Southeastern (SE), North-Central (NC) and Northeastern (NE) groups of stations are shown in Figures 5a, 5b, 5c, and 5d, respectively.

The *f-t* analysis enabled us to specify important properties of the recorded tsunami waves. The arrival of these waves is evident in almost all records (Figure 5). Moreover, for several stations the first arrivals were much more evident in the *f-t* plots than in the records themselves (in particular, for Patricia Bay, Point Atkinson and Nanaimo; Figures 3b, 4b and 5b). The *f-t* diagrams further allowed us to accurately estimate the dominant periods of tsunami waves at each site (see Table 2). The constructed *f-t* diagrams show that at some sites the oscillations had a monochromatic character, whereby one frequency, normally associated with the fundamental mode of the corresponding inner basin (inlet, bay or harbour), predominates (e.g. Winter Harbour, Tofino, Ucluelet, Port Alberni and Pruth Bay); at some other sites, there are two or more distinctive resonant frequencies.

The tsunami wave periods strongly varied from one site to another, but mostly were in the range of 12-60 min. The exceptions were Port Alberni and the entire Prince Rupert group, where dominant periods were over 100 min. Such long periods are typical for recorded tsunami waves at these two regions [cf. *Fine et al.*, 2009; *Rabinovich et al.*, 2019], as both Alberni Inlet and Dixon Entrance are well known to behave as low-pass filters that allow low frequency waves to propagate through while suppressing the transit of high frequency waves.

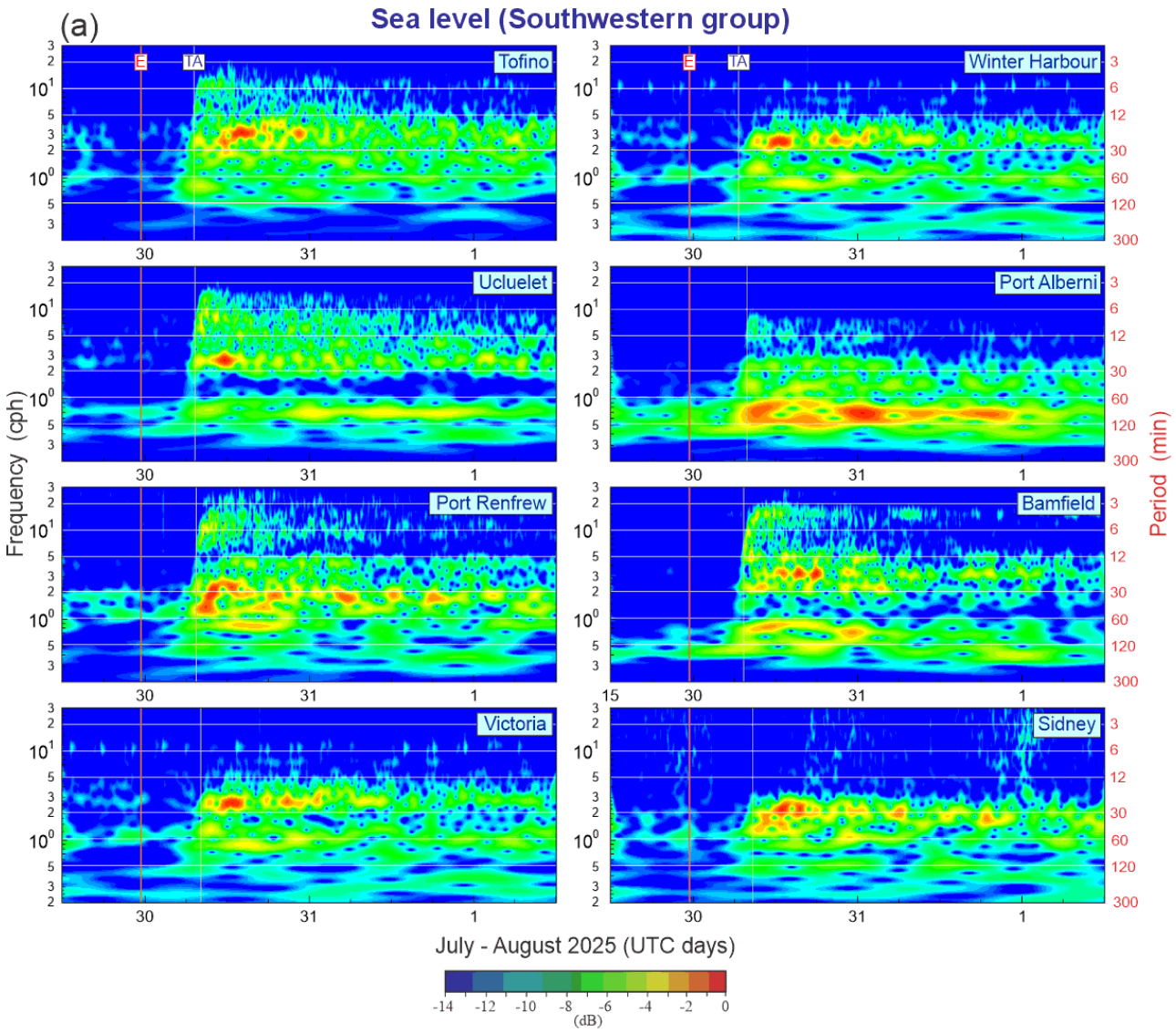

Figure 5. Frequency–time plots (*f–t* diagrams) derived using the 2025 Kamchatka tsunami CHS records shown in Figure 2. The solid vertical red lines labelled "E" indicate the time of the earthquake; the dashed thin vertical white lines labelled "TA" mark the tsunami arrival at the corresponding site. (a) Southwestern group.

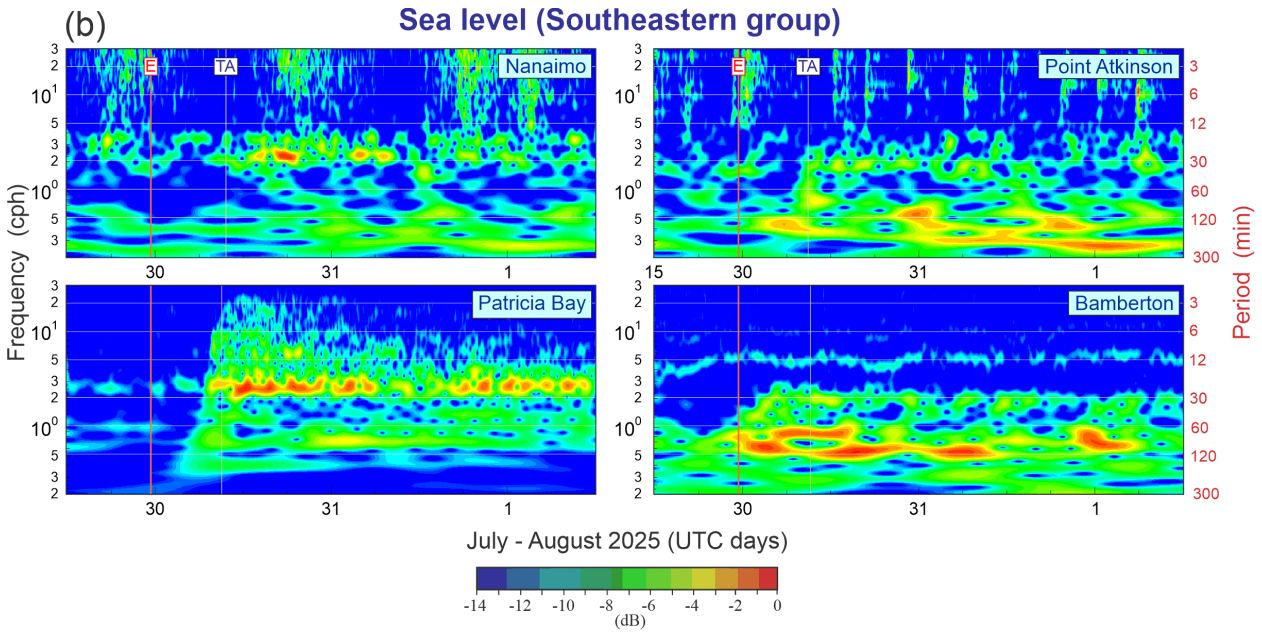

Figure 5. Continuation. (b) Southeastern group of stations.

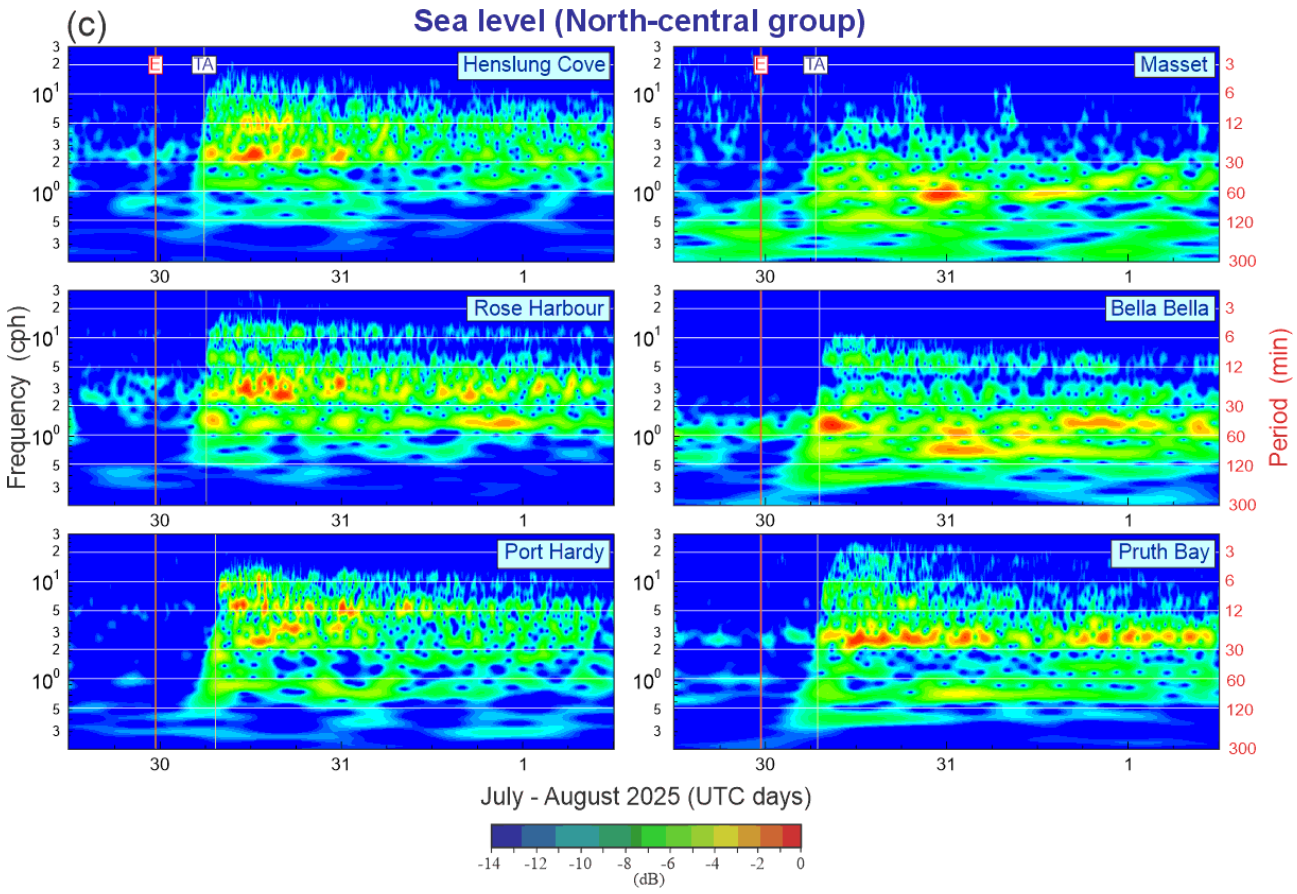

Figure 5. Continuation. (c) North-central group of stations.

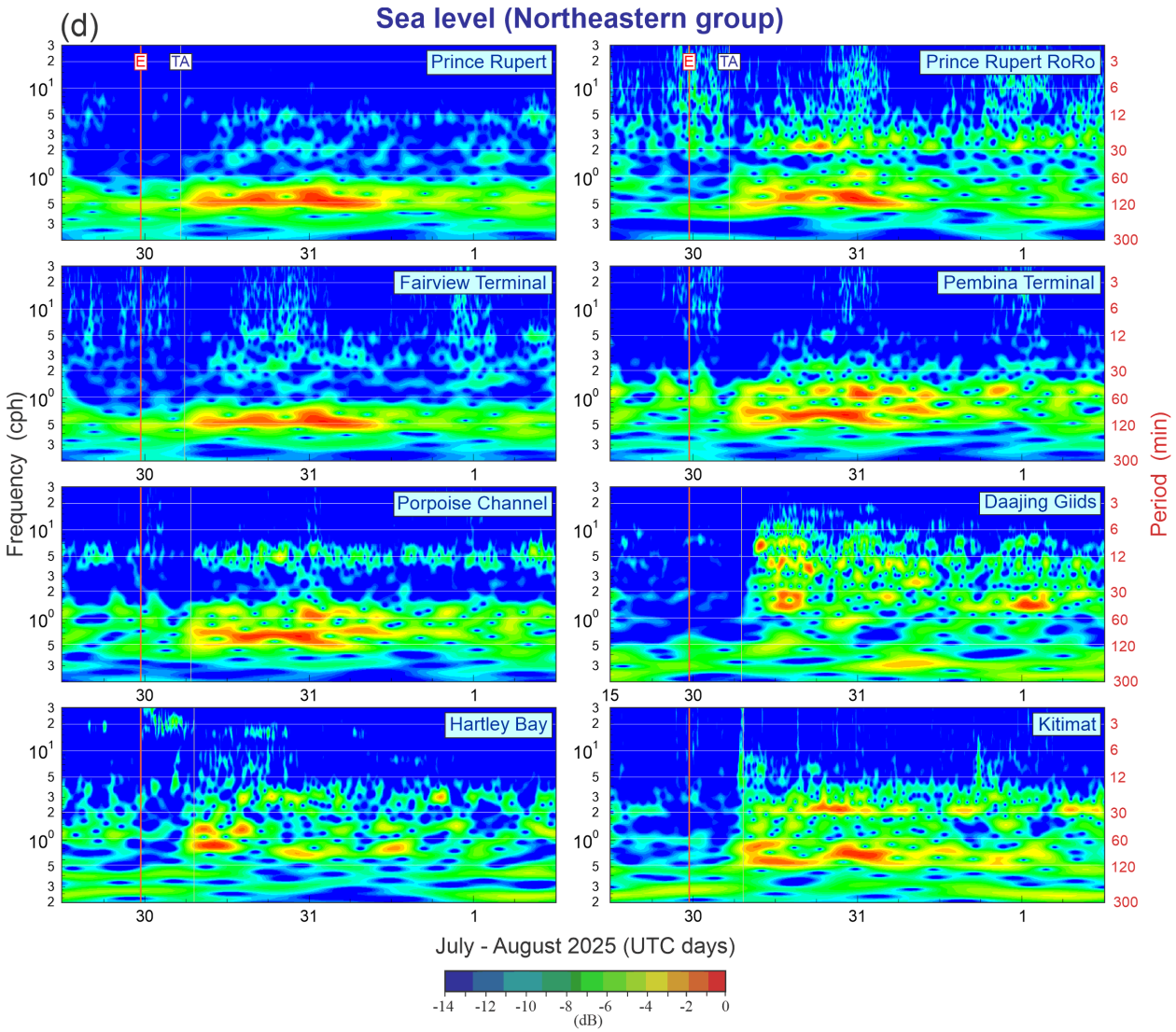

Figure 5. Continuation. (d) Northeastern group of stations.

The results of the *f-t* analysis are in good agreement with the resonant properties of the BC coast estimated by *Rabinovich et al.* [2025a]. As indicated in that report:

Long waves arriving from the open ocean can be strongly transformed and amplified by regional and local topography and bathymetry. The character of extreme sea level oscillations is determined by the specific geometry and physical features of the corresponding water basins, in particular, by the quality (Q) factors of these basins. Each closed or semi-closed basin has a set of natural (eigen) modes that are generated by external forcing and incoming open-ocean waves. Therefore, periods of observed tsunami waves are the same as those of regular background long waves recorded at the same site.

The coastline of British Columbia is complicated and has a diversity of topographic features, including islands, straits, bays, fjords and other waterways. These features strongly affect tsunami waves. While some of these features, such as the San Juan and Gulf islands,

shelter parts of the Salish Sea from destructive tsunami waves, others can resonantly amplify these waves.

This description characterizes well the properties of the 2025 Kamchatka tsunami waves along the BC coast. In particular, according to *Rabinovich et al.* [2025a], the highest wave amplification factor for all sites, $H_j(\omega)$ = 23.2, is found for Port Alberni. The corresponding resonant period $T_r \approx 103$ min is, as shown by *Fine et al.* [2009], associated with the fundamental (Helmholtz) oscillation mode of Alberni Inlet and is exactly what is observed for the 2025 tsunami. Moreover, the highest trough-to-crest wave height of ~94 cm was recorded at this station (Table 2) and the peak period was about 100 min (Figure 5a).

Similarly, the observed periods of the 2025 tsunami at the Prince Rupert group of stations, and at Kitimat (the NE group of stations), were 105-120 min, in close agreement with the resonant period T_r = 114 min for Prince Rupert as estimated by *Rabinovich et al.* [2025a] based on analysis of long background oscillation measurements at this site. Prevailing tsunami wave periods identified at other sites (Figure 5, Table 2) were also mostly in agreement with the resonant periods for the CHS sites determined by *Rabinovich et al.* [2025a].

In general, the 2025 tsunami oscillations at sites of the SW and NC groups, which are mainly located along regions of the coast most directly exposed to tsunami waves arriving from the open ocean, were significantly higher than those from the NE and SE groups, which were sheltered from the incoming waves.

4. RESULTS: OFFSHORE ONC DATA

Our examination of the 2025 Kamchatka tsunami near the coast of British Columbia also includes the open-ocean data from Ocean Networks Canada (ONC) and DART 46419[1]. These deep-ocean instruments are situated offshore of the coast of southwestern Vancouver Island at depths from 95 to 2815 m (Figure 6, Table 3).

Ocean Networks Canada is a continuously reporting ocean observatory network of physical, biological, and chemical sensors; it operates observatories in the deep ocean and coastal waters of Canada along the Pacific, Arctic and Atlantic coasts. The Canadian Northeast Pacific Underwater Net Experiments (NEPTUNE-Canada) is the Pacific segment of the ONC that is hosted and owned by the University of Victoria. Linked by an 825 km loop of fiber-optic cable with landfall at Port Alberni on Vancouver Island, NEPTUNE-Canada is enabling

[1] DART = Deep-ocean Assessment and Reporting of Tsunamis, is an effective network of deep-ocean stations designed for the continuous monitoring of tsunami waves in the open ocean and for early tsunami warning (cf. Rabinovich and Eblé 2015).

scientists to examine the structure and seismicity of the ocean crust, regional oceanic variability, deep-sea sedimentation, and various other geophysical processes [*Barnes et al.*, 2008]. The important feature of this network is that it is designed to provide realtime measurements of arriving tsunami waves as they cross the flat abyssal plain region of Cascadia Basin and propagate over the continental slope and shelf. This system was effectively used to record the 2009 Samoa [*Thomson et al*., 2011], 2010 Chilean [*Rabinovich et al.*, 2013], 2011 Tohoku [*Fine et al.*, 2013], 2012 Haida-Gwaii [*Fine et al.*, 2015], 2018 Alaska-Kodiak [*Wang et al.*, 2020], and 2021 South Sandwich Islands [*Rabinovich et al.*, 2025b] tsunamis, as well as the 2016 meteotsunami associated with typhoon Songda [*Rabinovich et al.*, 2023].

In total, we were able to download 11 quality ONC bottom pressure time series located in five nodes: Endeavour, Cascadia Basin, Clayoquot Slope, Barkley Canyon and Folger Passage (Figure 6, Table 3). Two Endeavour stations, Endeavour Main and Endeavour Main South, are located less than 10 m from each other, so that the instruments recorded practically identical tsunami signals. The stations of the Endeavour group create a cluster of stations shown in the inset in Figure 6. Two Cascadia Basin stations, Northeastern (NE) and Southeastern (SE), are situated approximately 26 km from each other (Table 4).

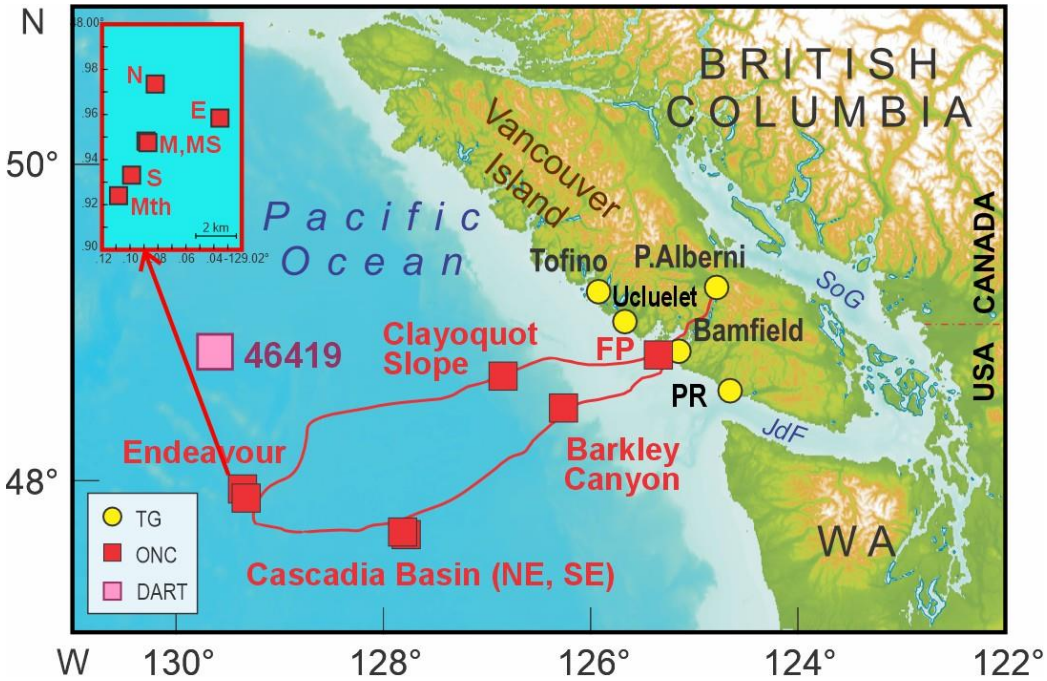

Figure 6. (a) Map of Vancouver Island, British Columbia, showing locations of DART 46419 and 11 offshore cable ONC bottom pressure stations. Six stations of the Endeavour group are shown in the inset. Also are indicated five CHS tide gauges (TG) situated in this region. Abbreviations: WA = Washington State (USA), PR = Port Renfrew, SoG = the Strait of Georgia, JdF = Juan de Fuca Strait; FP = Folger Passage, six ONC Endeavour stations: N = North, E = East, M = Main, MS = Main South, S = South and Mth = Mothra.

The DART system operates in two modes: (1) the *Standard (normal) operating mode* with four samples per hour, and (2) the *Event mode* with data collected over a few minutes at 15-s resolution before changing to transmissions at 1-min averages [*Mungov et al.*, 2013; *Rabinovich and Eblé*, 2015]. Event mode is triggered either (1) manually (by an operator) or (2) automatically with passage of a wave having an amplitude higher than 3 cm. A typical length of Event mode records is from a couple of hours to one day. Data from DART 46419 used in the present study were from the Event mode and had a length of 11 hours, from 05:00 to 16:00 UTC on 30 July.

Table 3. Principal information for DART 46419 and ONC bottom pressure cable stations positioned offshore of Vancouver Island, British Columbia, that were used to examine the 2025 Kamchatka tsunami. (See Figure 6 for locations.)

Node	Station	Coordinates		Depth (m)
		Latitude (°N)	Longitude (°W)	
DART	46419	48.8150	-129.6230	2815
Endeavour Ridge	East	47.9584	-129.0356	2321
	North	47.9735	-129.0819	2152
	South	47.9331	-129.0988	2228
	Main	47.9486	-129.0987	2195
	Main South	47.9482	-129.0988	2193
	Mothra	47.9240	-129.1082	2276
Cascadia Basin	Northeast	47.9062	-127.6205	2640
	Southeast	47.6698	-127.5934	2639
Clayoquot Slope	Bullseye	48.6709	-126.8480	1257
Barkley Canyon	Upper Slope	48.4268	-126.1747	393
Folger Passage	Folger Passage	48.8140	-125.2810	95

The data analysis procedure for offshore records of the 2025 Kamchatka tsunami was the same as for the coastal tide gauge records (Section 2). The data were verified and corrected, the tides were estimated and subtracted, and the residual series were high-pass filtered with a 4-h Kaiser-Bessel (KB) window [cf. *Thomson and Emery* 2024] to suppress low-frequency oscillations associated with atmospheric processes. These filtered ONC time series (which have the same length as coastal records) then were used to construct the plots of tsunami records (Figures 7-8) and their *f-t* diagrams (Figure 9), and to estimate statistical characteristics of the recorded tsunami waves (Table 4). The records for stations Endeavour Main and Endeavour South were found to be the same; therefore, the latter record and the corresponding *f-t* are not shown in Figures 7-9.

Table 4. Parameters of the Kamchatka tsunami of 29 July 2025 recorded by DART 46419 and ONC bottom cable stations offshore of southwestern Vancouver Island, British Columbia. All arrival times and times of the maximum waves (in UTC hours) are related to 30 July 2025. (Earthquake M_w 8.8 at 23:25 UTC on 29 July 2025).

Station (Depth)	First wave			Max waves			Period[+] (min)
	Arrival time (UTC)	Travel time (hh:mm)	Amplitude (cm)	Max amplitude (cm)	Time (UTC) of max amplitude	Max wave height (cm)	
DART 46419 (2815 m)	05:59	06:34	+4.9	4.9	06:14	9.0	38,28,9,7
Endeavour East (2321 m)	06:07	06:42	+4.8	4.8	06:20	10.1	38, 20, 9
Endeavour North (2152 m)	06:07	06:42	+4.8	4.8	06:20	9.9	38, 20, 9
Endeavour South (2228 m)	06:06	06:41	+4.9	4.9	06:19	10.1	38, 20, 9
Endeavour Main (2195 m)	06:06	06:41	+4.3	4.3	06:19	10.0	38, 20, 9
Endeavour Main South (2193 m)	06:06	06:41	+4.9	4.9	06:19	10.2	38, 20, 9
Endeavour Mothra (2276 m)	06:06	06:41	+4.9	4.9	06:19	10.2	38, 20, 9
Cascadia Basin NE (2640 m)	06:19	06:54	+4.7	4.7	06:31	9.2	28, 20, 9
Cascadia Basin SE (2639 m)	06:19	06:54	+4.7	4.7	06:31	8.9	28, 20, 9
Clayoquot Slope Bullseye (1257 m)	06:24	06:59	+6.0	6.0	06:37	10.2	48, 115, 18
Barkley Canyon Upper Slope (393 m)	06:31	07:06	+7.1	7.1	06:43	13.7	38, 28, 20, 9
Folger Passage (95 m)	07:08	07:43	+11.6	13.3	13:01	25.7	24, 47, 85

[+] Periods are given in the importance order.

In general, the tsunami analyses for all ONC stations lead to consistent results. The first wave arrived at the stations of the Endeavour group at 06:06 - 06:07 UTC, which is approximately 6 h and 41-42 min after the main earthquake shock. These times are 60-70 min earlier than the tsunami waves that arrived at the nearby coast of Vancouver Island (stations Tofino, Ucluelet and Bamfield; see Table 2), once again indicating that the ONC stations can

be effectively used for early tsunami warning. About 13 min later, the tsunami waves arrived at the stations of the Cascadia Basin group. The eight stations from these two groups are all deep-water stations with depths of 2152-2640 m (Table 3). Most of the parameters of the recorded tsunami waves were very similar. The first wave was positive, had the maximum amplitude (4.7-4.9 cm) of the wave train, maximum trough-to-crest wave heights of 8.9-10.2 cm, and observed periods of 38 (28), 20 and 9 min (Table 4, Figures 7-9).

As the waves approached the coast, the tsunami amplitudes and maximum wave heights began to gradually increase with decreasing depth, becoming +6.0 and 10.2 cm at Clayoquot Slope, +7.1 and 13.7 cm at Barkley Canyon, and +11.6 and 25.7 cm at Folger Passage. The wave heights at Folger Passage are different from all the others: in that it is the shallowest (95 m) site, the closest site to the coast and measured the highest tsunami oscillations, with periods significantly different from those at the other ONC stations. It appears that these periods are determined by the local resonant properties of the shelf and adjacent coastal geometry rather than by the spectral properties of the source. Similar features of sea level oscillations at Folger Passage, mismatched with those at the other ONC stations, were observed during the October 2016 meteotsunami generated by typhoon Songda [*Rabinovich et al.*, 2023].

The Folger Passage ONC station is located only 11 km offshore from a coastal tide gauge station at Bamfield. The tsunami signal at Bamfield arrived 12 min later than at Folger Passage (07:20 and 07:08 UTC, respectively); the maximum tsunami amplitude and height at Bamfield were only slightly greater than at Folger Passage, with Bamfield versus Folger Passage of 13.6/29.7 cm and 11.6/25.7 cm, respectively (Tables 2 and 4). Significant amplification of arriving tsunami waves occurred further inshore at Port Alberni (51.0/94.0 cm), situated at the head of long and narrow Alberni Inlet (Figure 6).

In addition to the coastal tide gauge and ONC records, we also examined the Event mode de-tided record at DART 46419 (Figure 10a). The estimated parameters of the 2025 tsunami waves at this station are quite similar to those for the ONC stations of the Endeavour group (Table 4). In particular, tsunami waves arrived at DART 46419 at 05:59 UTC, i.e., 10 min earlier than at stations of the Endeavour group, while the maximum wave amplitudes and heights were almost the same as at the deep-water ONC stations. Similarly, the observed periods of the tsunami waves (Figure 10b) were very similar to those at the ONC stations (except Folger Passage). It appears that the periods at all stations located beyond the shallow-water shelf zone (38, 28, 9 and 7 min), which are quite mutually consistent, are associated with the frequency properties of the source.

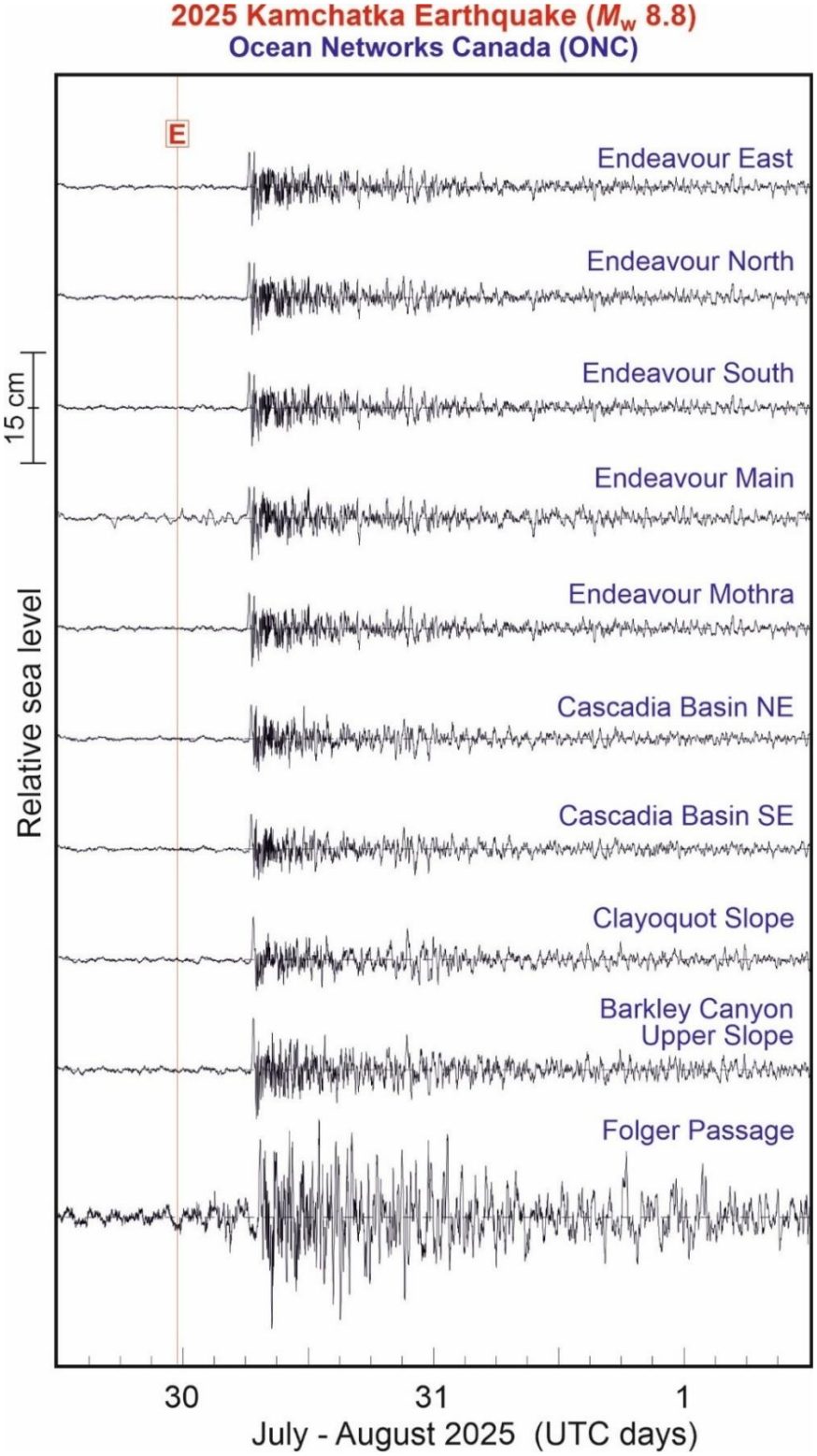

Figure 7. De-tided and high-pass filtered (4-hour Kaiser-Bessel window) 3-day records of the 2025 Kamchatka tsunami at ten ONC stations offshore of Vancouver Island, British Columbia. The solid vertical red line labelled "E" indicates the time of the earthquake. The individual records are shifted in the vertical relative to each other; a vertical scale for the waveforms is presented along the left axis. (a) Southwestern group of stations.

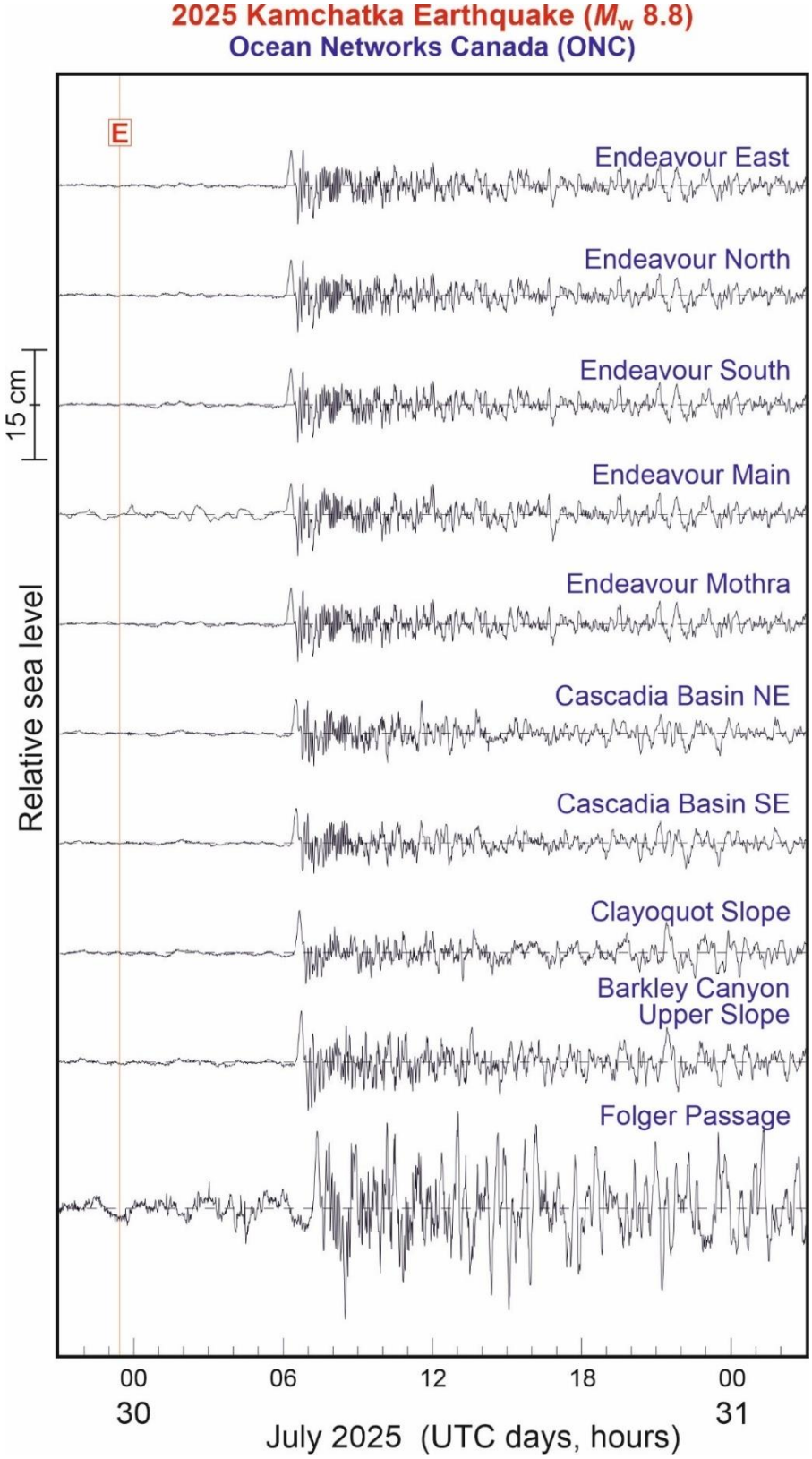

Figure 8. The same as in Figure 7 but for 1.25-day segments between 21:00 UTC on 29 July and 03:00 UTC on 31 July 2025.

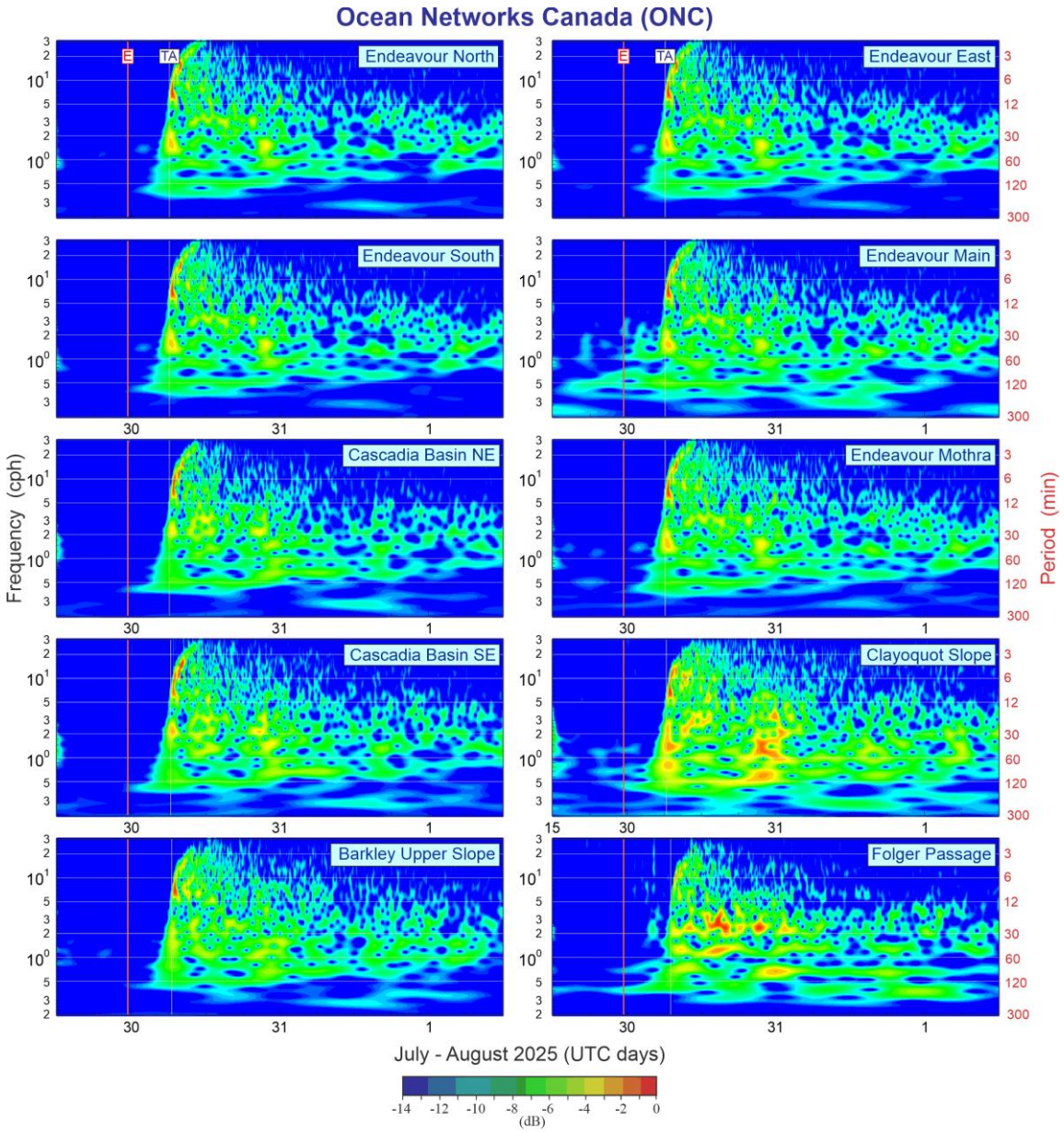

Figure 9. Frequency–time plots (*f–t* diagrams) derived using the 2025 Kamchatka tsunami ONC offshore records shown in Figure 7. The solid vertical red lines labelled "E" indicate the time of the earthquake; the dashed thin vertical white lines labelled "TA" mark the tsunami arrival at the corresponding sites.

An important feature of all of the open-ocean 2025 Kamchatka tsunami records (ONC and DART 46419) is a leading small-amplitude negative-phase semiwave. *Eblé et al*. [2015] demonstrated that such a feature is common for all strong distant tsunamis. In particular, they found it in 15-s DART records of trans-Pacific tsunamis following the 2010 Chile (Maule), 2011 Tohoku, 2012 Haida Gwaii, and 2014 Chile (Iquique) earthquakes. Observations investigated during each of the four events indicates an increase in this effect with increasing distance from the tsunami source. As was shown by *Allgeyer and Cummins* [2014], *Watada*

et al. [2014] and *Watada* [2023], this frontal negative wave is mostly related to the elastic properties of the Earth and tsunami mass loading on the sea bottom. A typical amplitude of this "semiwave" in the 2025 Kamchatka ONC/DART records was about 0.8 cm (Figures 8 and 10a).

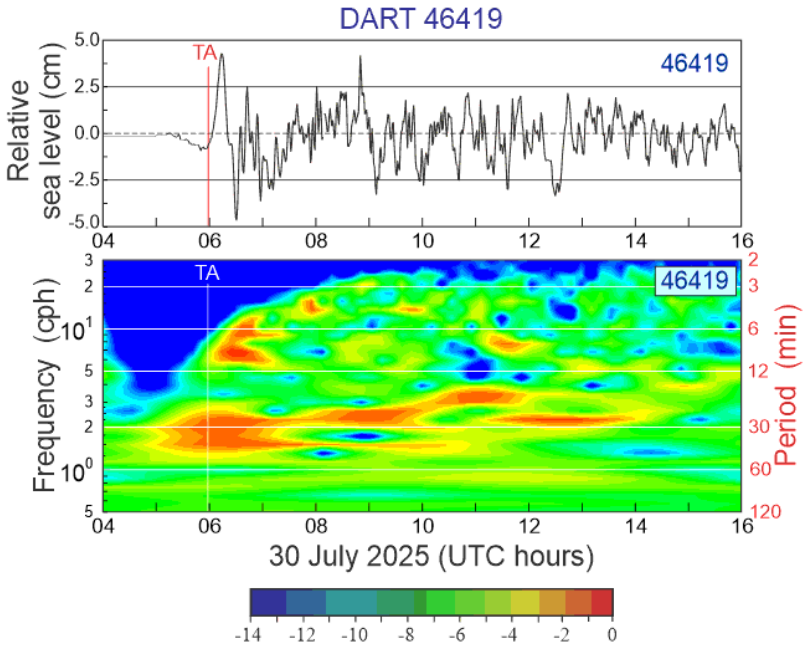

Figure 10. (a) De-tided 12-hour records of the 2025 Kamchatka tsunami measured at DART 46419 offshore of Vancouver Island; wave heights are in cm; and (b) Frequency–time plots (*f*–*t* diagrams) derived from this record. The solid vertical red (white) lines labelled "TA" mark the tsunami arrival at the corresponding site.

5. COMPARISON OF THE 1952 AND 2025 KAMCHATKA TSUNAMIS

As indicated in the Introduction, the source area of the 2025 Kamchatka earthquake (M_w 8.8) almost coincided with that of the 1952 Kamchatka earthquake (M_w 9.0), which was one of the greatest ever instrumentally recorded earthquakes. Both the 1952 and 2025 earthquakes generated major trans-Pacific tsunamis (Figure 6) that were observed throughout the entire Pacific Ocean. The analog paper records of the 1952 tsunami were collected and published by *Weeks and Studds* [1953]; the more than 600 digital 2025 coastal tsunami records continue to be examined.

Five tide gauges recorded the 1952 tsunami on the coast of British Columbia: Prince Rupert, Kitimat, Alert Bay, Tofino and Victoria [*Rabinovich et al.*, 2019]. The Alert Bay station is no longer working and was not working at the time of 2025 event, but the other four gauges were among the 26 CHS tide gauges that recorded the 2025 tsunami. Thus, there were four CHS stations that recorded both the 1952 and 2025 tsunamis. This made it possible to

compare the principal statistical parameters of the two tsunamis recorded at the same sites (Table 3).

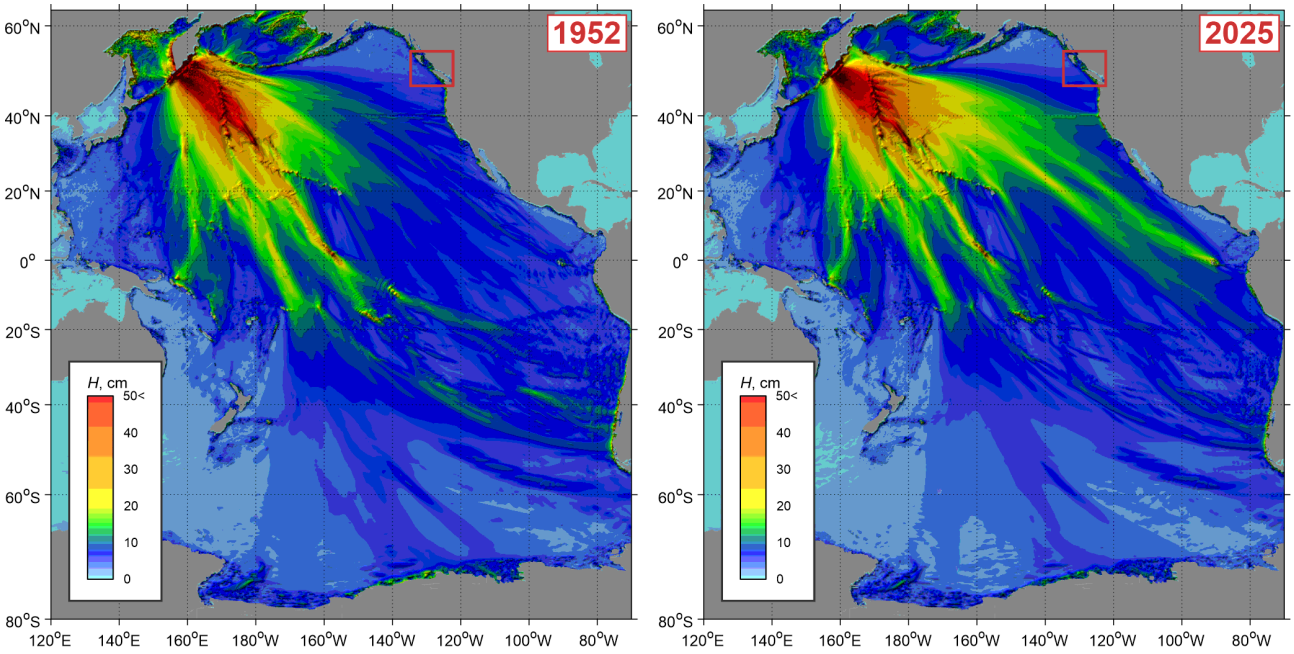

Figure 11. Numerically simulated maximum wave amplitudes for the 1952 and 2025 Kamchatka tsunamis for the Pacific Ocean. The red boxes frame the area of British Columbia examined in the present study.

The tsunami travel times for the 1952 and 2025 events were quite similar. In the case of the two northern stations, Prince Rupert and Kitimat, the 1952 tsunami took 12 and 4 min longer, respectively, to reach the sites. In contrast, the propagation times to Victoria were almost identical, while to Tofino the 2025 waves took 12 min longer than the 1952 waves (Table 2). These small differences (up to 2.5%) appear to be related to minor differences in the exact position and orientation of the two sources. As might be expected, the observed periods of the recorded waves for each site for the 1952 and 2025 events are similar. Two additional 2025 tsunami periods, 75 min at Tofino and 67 min at Victoria, are most probably related to the much higher accuracy of the 2025 digital instruments compared to the 1952 analog tide gauges (the 1952 paper records were digitized prior to analysis by *Rabinovich et al.*, 2019), which made it possible to identify several minor oscillations.

The 1952 earthquake was slightly more intense than the 2025 earthquake (M_w 9.0 and 8.8, respectively); therefore, it is not unexpected that the 1952 tsunami waves were higher than the 2025 waves. We compared three parameters of the two events: the first wave amplitudes, maximum wave amplitudes and maximum trough-to-crest wave heights (Table 3). The mean

ratio for all three parameters and for all four stations was 1.60. It is, therefore, logical to assume that the same 1952/2025 tsunami wave ratio applies to the entire Pacific Ocean.

Table 5. Parameters of the Kamchatka tsunamis of 4 November 1952 and 29 July 2025 recorded at four CHS tide gauges on the coast of British Columbia (Main shocks are M_w 9.0 at 16:58 UTC and M_w 8.8 at 23:25 UTC, respectively).

Station	Year	First wave		Maximum wave		Period (min)	Ratio 1952/2025		
		Travel time (h:mm)	Amplitude. (cm) Sign	Amplitude. (cm)	Height (cm)		First	Max Ampl.	Max height
Prince Rupert	1952	7:45	+7.0	11.8	23.7	110	2.26	1.48	1.48
	2025	7:33	+3.1	8.0	16.0	120			
Kitimat	1952	8:19	+5.5	8.5	17.0	30, 100	1.38	1.73	1.95
	2025	8:15	+4.0	4.9	8.7	28, 110			
Tofino	1952	7:32	+26.2	33.7	77.0	22	1.68	1.55	1.73
	2025	7:43	+15.6	21.8	44.5	19, 75			
Victoria	1952	8:42	+6.0	18.0	38.8	25	1.00	1.43	1.62
	2025	8:43	+6.0	12.6	24.0	23, 67			

6. NUMERICAL MODELLING

To numerically simulate the 2025 Kamchatka tsunami, we applied the shallow-water linear finite-difference model of *Fine et al.* [2013, 2015], which is similar to the well-known TUNAMI model [*Imamura*, 1996]. This model was successfully used to compute a great number of tsunamis, including the 2018 Alaska-Kodiak [*Wang et al.*, 2020], the 2017 and 2022 Mexican [*Zaytsev et al.*, 2023], the 2005 Indian Ocean [*Medvedeva and Rabinovich*, 2025], the 2024 Noto Peninsula [*Tsukanova et al.,* 2025] and the 2021 South Sandwich Islands [*Rabinovich et al.*, 2025b] tsunamis.

The USGS moment tensor parameters of the 2025 Kamchatka earthquakes were as follows: Moment = $2.221 \cdot 10^{-22}$ N·m, M_w = 8.83, Lat = 59.495°N, Long = 160.240°E, depth = 21.5 km, NP1: strike = 198°, dip = 18°, and rake = 51°; NP2: strike = 58°, dip = 76°, and rake = 101° (https://earthquake.usgs.gov/earthquakes/eventpage/us6000qw60/moment-tensor). For our numerical model, we used a slightly modified version of the USGS finite fault, Version 4

model) that was based on the tensor nodal plane, with strike = 215.0° and dip = 6.5°/17°/28°. The 15-arcsec global bathymetry dataset GEBCO 2025 (https://www.gebco.net), subsampled to a coarser grid with a spatial resolution of 1 arcmin, was applied for the numerical model domain for the 2025 Kamchatka tsunami. The time step was calculated automatically to satisfy the CFL criterion. To validate and fine-tune the tsunami source model, we made use of data from six DART stations closest to the source: 21413, 21414, 21415, 21418, 21419 and 46408 (all located in the northwestern Pacific Ocean).

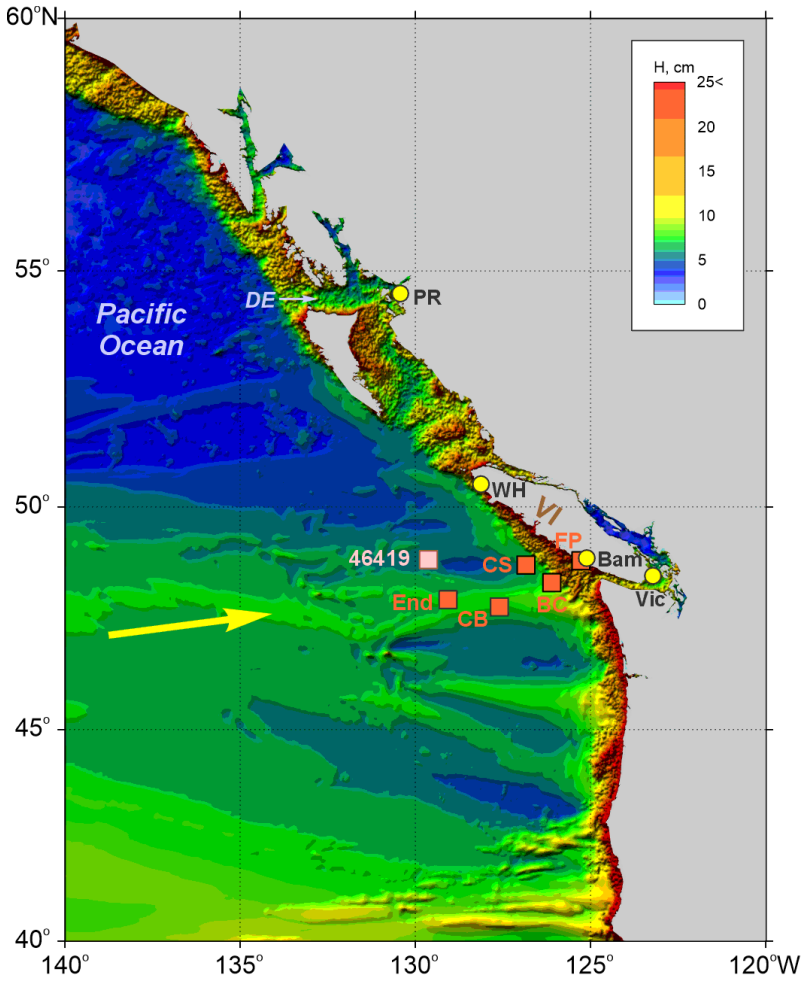

Figure 12. Numerically simulated maximum wave amplitudes for the 2025 Kamchatka tsunamis for the northeast Pacific Ocean. The orange squares show the locations of the ONC node stations, the pink square indicates the position of DART 46419, the yellow circles designate four coastal tide gauges, while the orange arrow denotes the direction of arriving tsunami waves. Abbreviations: DE = Dixon Entrance, VI = Vancouver Island, PR = Prince Rupert, WH = Winter Harbour, Bam = Bamfield, Vic = Victoria, End = Endeavour, CB = Cascadia Basin, CS = Clayoquot Slope, BC = Barkley Canyon, and FP = Folger Passage.

The results of the numerical simulation of the 2025 Kamchatka tsunami for the entire Pacific Ocean are shown in Figures 1 and 11. The main energy of this tsunami went to the southwest in the direction of the Hawaiian Islands and Chile. In the present study, we focused on the northeastern part of the Pacific Ocean, i.e., to the region adjacent to coastal British Columbia. In the case of this region, the 2025 tsunami arrived from the west and west-southwest (Figure 12).

As shown in Section 4, the tsunami was clearly recorded by the ONC stations (Figures 7 and 8) and by DART 46419, located nearby (Figure 10). Numerically simulated tsunami waves arriving at this region are presented in Figure 12, while computed and observed tsunami waveforms for DART 46419 and five node stations are shown in Figure 13. The simulated and recorded tsunami waveforms are in good agreement. The model reproduces correctly not only the first but also the following trains of waves, including their amplitudes and periods, as well as the general amplification of tsunami waves approaching the coast. The records presented include about 8 hours of measured and simulated waves and show that, for the four deepwater stations (DART 46419, Endeavour Main, Cascadia Basin NE and Clayoquot Slope), the agreement is almost perfect for this entire period. The results began to differ slightly only for Barkley Canyon (water depth 393 m) and for Folger Passage (depth 95 m). It is evident that for these near coast stations, we need to use a finer grid and better spatial resolution.

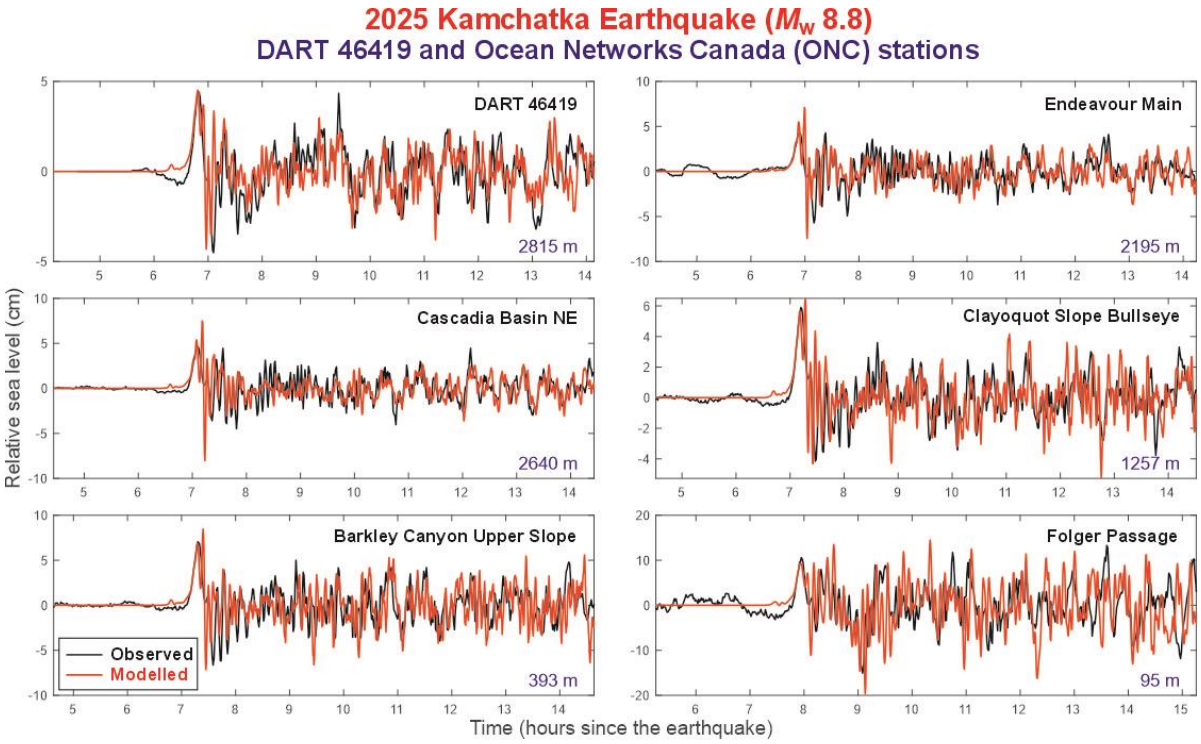

Figure 13. Numerically simulated and observed tsunami waveforms of the 2025 Kamchatka tsunami for DART 46419 and five ONC open-ocean stations related to five different nodes (see Figure 6 for station locations). The station depths are indicated.

We also computed tsunami waveforms for five stations from the ONC Endeavour group and one from Cascadia Basin Southeast. All these stations are deep-water (depths from 2152 to 2639 m) and agreement for all stations was almost perfect for the entire 8-hour period (Figure 14).

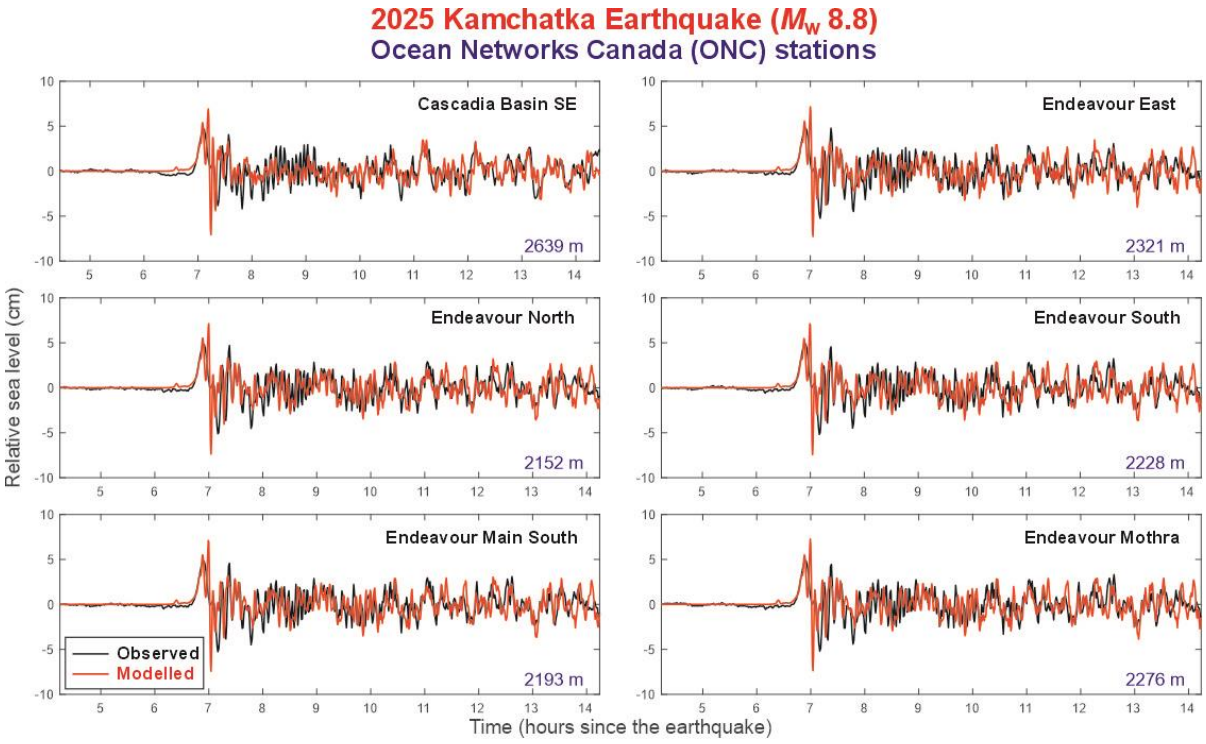

Figure 14. Numerically simulated and observed tsunami waveforms of the 2025 Kamchatka tsunami for the ONC Cascadia Basin Southeast station and five ONC Endeavour node stations (see Figure 6 for station locations). The station depths are indicated.

Additionally, we selected four coastal stations for comparison with the modeled waveforms: Victoria, Bamfield and Winter Harbour along the coast of Vancouver Island and Prince Rupert, on the northwestern coast of mainland British Columbia (Figure 12). The properties of tsunami records at these stations were discussed in Section 3 (see Figures 3-5 and Table 2). Mostly they are determined by local topography of the respective sites. In particular, Dixon Entrance, which is the main gate for tsunami waves reaching Prince Rupert, acts as a low-pass filter, strongly suppressing high-frequency waves but allowing low frequencies to pass through freely. This feature is correctly reproduced by our numerical modelling (Figure 15). However, the computed period of 120 min is slightly higher than the observed period of 110 min (Table 2). In contrast, the computed period for Winter Harbour is slightly lower than the observed period. In general, the simulated waveforms correctly reproduce some important properties of the actual coastal tsunami records, but the agreement is significantly worse than for the open-ocean records. This is expected taking into account that we used a relatively coarse numerical grid with ~3.7 km spatial resolution that is appropriate for the deep ocean but not for the coastal zone. As indicated by *Fine et al.* [2018], accurate numerical simulation of tsunami waves in the rapidly shoaling regions of the west coast of British

Columbia requires setting up a model domain as a series of nested grids of ever finer spatial and temporal resolution. The use of nested grids of smaller cell dimensions and time steps makes it possible to resolve tsunami wave configurations as they propagate into the shallow coastal regions.

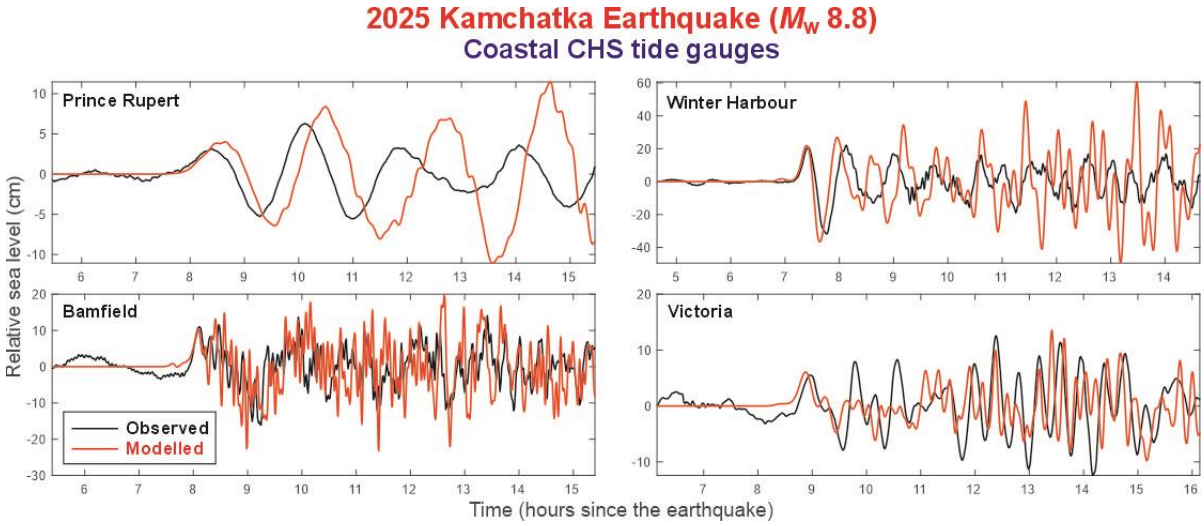

Figure 15. Numerically simulated and observed tsunami waveforms of the 2025 Kamchatka tsunami for coastal CHS tide gauges located along the coast of British Columbia (see Figure 2a for station locations).

7. SUMMARY AND CONCLUSIONS

The Kamchatka tsunami of 29 July 2025 was one of the strongest trans-Pacific tsunamis ever recorded, comparable with the 1946, 1952, 1957, 1960, 1964, 2010 and 2011 events. Waves from the event spread over the entire Pacific Ocean and were clearly recorded on the coast of British Columbia. To examine the 2025 tsunami at this coast, 27 CHS tide gauge records were selected. Tsunami waves were evident in 26 of the records. The tsunami was measured not only on the oceanic coast of Vancouver Island, at Henslung Cove and Rose Harbour, but also at such sheltered sites as Point Atkinson, Sidney, Patricia Bay, Nanaimo, Hartley Bay and Kitimat.

The first waves arrived at Henslung Cove 6 h and 24 min after the main shock and then, 20-50 min later, at Rose Harbour, Winter Harbour and Masset. Roughly 70 min after that, the waves arrived at the group of Prince Rupert stations in the north and ~80-90 min later at the central and northwestern coasts of Vancouver Island. Approximately 3-4 hours after the first waves reached the coast of northwestern British Columbia, tsunami waves arrived at stations

located in the Strait of Georgia (Point Atkinson and Nanaimo) and in Saanich Inlet (Patricia Bay and Bamberton).

The maximum wave amplitude on the BC coast of 51 cm (wave height, 94 cm) was observed at Port Alberni. This is not unexpected in that, according to *Rabinovich et al.* [2025], the site is characterized by the strongest resonant properties and the highest amplification factor for the BC coast. The maximum wave height at Winter Harbour was54 cm, and at Tofino, Ucluelet and Henslung Cove, 40-45 cm. The smallest identified tsunami waves (3.5-4 cm) were observed at Point Atkinson and Nanaimo.

The 2025 Kamchatka tsunami was recorded by 11 ONC stations and by DART 46419 located offshore of Vancouver Island. The first wave arrived at the DART 6 h and 34 min after the earthquake and then 7-8 min later at six stations of the Endeavour group. These are 60-70 min earlier than the waves that reached the nearby coast of Vancouver Island, once again indicating that the DART and the ONC stations can be effectively used for the early tsunami warning. Parameters of the recorded waves at the six Endeavour stations and other five ONC stations were in good agreement: the first wave was positive, and the highest waves had maximum amplitudes of +4.7 – 4.9 cm at the 9 deep-water stations (2142 – 2815 m), +6.0 and 7.1 cm at two ONC stations located at depths of 1257 and 393 m, respectively. The waves reached 11.6 cm at Folger Passage (water depth 95 m) - the station located only 11 km offshore, which recorded the tsunami signal 12 min earlier than at Bamfield. The observed periods at all offshore stations, except Folger Passage, were 38 (28), 20 and 9 min that probably were associated with the spectral properties of the source area. In contrast, the measured wave periods at Folger Passage of 24, 47 and 85 min were probably determined by the local resonant properties of the shelf and adjacent coast.

One of the most intriguing aspects of the present study involves the comparison of two Kamchatka events: the 2025 tsunami induced by a M_w 8.8 earthquake and the 1952 tsunami produced by one of the greatest historical earthquakes, with a momentum magnitude M_w 9.0. The source areas of these two earthquakes were nearly coincided. Both generated tsunamis that were trans-Pacific and were clearly recorded on the coast of British Columbia. Four tide gauges - Prince Rupert, Kitimat, Tofino and Victoria – measured both events. Comparison of these records show that the tsunami travel times for the 1952 and 2025 events were quite similar, such that the differences in these times for the same stations did not exceed 12 min and the observed periods of the recorded waves for each site for the two events were also alike. The ratio of the recorded wave heights, 1952/2025, was approximately 1.60, in agreement with the

fact that the 1952 earthquake was slightly stronger than the 2025 earthquake (M_w 9.0 and 8.8, respectively).

Our reconstruction and numerical modelling of the two tsunamis confirm the 1952/2025 wave height ratio and provide realistic results for the 1952 and 2025 tsunami runups and inundations along the coasts of the North Kuril Islands and southeastern Kamchatka, as well as realistic far-field simulations for the North American and Chilean tsunami waveforms. In general, the absence of infrastructure damage and fatalities from the major 2025 tsunami demonstrates that the difference in the consequences of the 1952 and 2025 events is *clearly due to the impressive progress achieved in seventy years of tsunami science, and operational services!* For example, the town of Severo-Kurilsk, which was destroyed by the 1952 tsunami, was moved uphill to a tsunami safe zone. In addition, the construction design of buildings in Petropavlovsk-Kamchatsky (the capital of Kamchatka Krai) and other towns of this region was significantly improved to make the structures "seismically-resistant". Even more important than improved construction methods is *education*. People in the Kamchatka and Kuril regions, as well as in other coastal areas of the Pacific Ocean, had learned well the dangers posed by tsunami waves and knew what to do when the tsunami warnings were issued at the time of the 2025 event.

To numerically simulate the 2025 Kamchatka tsunami, we applied the shallow-water linear finite-difference model of *Fine et al.* [2013, 2015, 2018]. The computed tsunami waveforms for DART 46419 and 11 ONC stations were in near perfect agreement with the actual Kamchatka tsunami records at these stations. We also simulated the 2025 tsunami records for four coastal stations, Victoria, Bamfield, Winter Harbour and Prince Rupert. The results were satisfactory but certainly worse than for the open-ocean stations. Much better spatial resolution and nested grids of ever finer spatial and temporal resolution could rectify this situation. The use of nested grids of smaller cell dimensions and time steps makes it possible to resolve tsunami wave configurations as they propagate into the shallow coastal regions.

ACKNOWLEDGEMENTS

The authors would like to acknowledge the CHS staff for their invaluable help in preparation of the CHS tide gauge time series, which were used to identify and examine the tsunami signal, and personally Kevin Jones for his reconstitution of the history of CHS tide gauge measurements. The authors also thank Isaac Fine for his help with numerical modelling of 2025 Kamchatka tsunami and Fred Stephenson for his careful editing of the report. The final

version was reviewed for publication by Neil Dangerfield of the Institute of Ocean Sciences (Fisheries and Oceans, Canada).

REFERENCES

Allgeyer, S., Cummins, P. (2014), Numerical tsunami simulation including elastic loading and seawater density stratification. *Geophysical Research Letters*, 41(7), 2368–2375. https://doi.org/10.1002/2014GL059348.

Andrews, R.G. (2025), Why the Russian earthquake didn't cause a huge tsunami? *Scientific American*. Retrieved 2 August 2025.

Barnes, C., Best, M., Johnson, F., Phibbs, P., and Pirenne, B. (2008), Transforming the ocean sciences through cabled observatories, *Marine Technology Reporter*, 30–36, Oct.

Eblé, M.C., Mungov, G., Rabinovich, A.B. (2015), On the leading negative phase of major 2010-2014 tsunamis, *Pure and Applied Geophysics*, 172 (12), 3493-3508; doi 10.1007/s00024- 01.

Fine, I.V., Cherniawsky, J.Y., Rabinovich, A.B., and Stephenson, F.E. (2009), Numerical modeling and observations of tsunami waves in Alberni Inlet and Barkley Sound, British Columbia, *Pure and Applied Geophysics*, *165*(11/12), 2019-2044.

Fine, I.V., Kulikov, E.A. (2011), Calculation of sea surface displacements in a tsunami source area caused by instantaneous vertical deformation of the seabed due to an underwater earthquake, *Computational Technologies*, 16, 111–118 [in Russian].

Fine, I.V., Kulikov, E.A., Cherniawsky, J.Y. (2013), Japan's 2011 tsunami: Characteristics of wave propagation from observations and numerical modelling, *Pure and Applied Geophysics*, 170, 1295–1307. https://doi.org/10.1007/s00024-012-0555-8.

Fine I.V., Thomson R.E. (2013), A wavefront orientation method for precise numerical determination of tsunami travel time, *Natural Hazards and Earth System Sciences*, 13(11), 2863–2870. https://doi.org/10.5194/nhess-13-2863-2013.

Fine, I.V., Cherniawsky, J.Y., Thomson, R.E., Rabinovich, A.B., Krassovski, M.V. (2015), Observations and numerical modeling of the 2012 Haida Gwaii tsunami off the coast of British Columbia, *Pure and Applied Geophysics*, 172 (3-4), 699-718; doi: 10.1007/s00024-014-1012-7.

Fine, I.V., Thomson R.E., Lupton L.M., and S. Mundschutz (2018), Numerical modelling of a Cascadia subduction zone tsunami at the Canadian Coast Guard Base at Victoria, British Columbia. Can. Tech. Rep. Hydrogr. Ocean Sci. 324, 34 p.

Imamura, F. (1996), Review of tsunami simulation with a finite difference method. In: *Long-Wave Run-up Models* (Eds. H. Yeh, P. Liu, and C. Synolakis), World Scientific, Singapore, pp. 25-42.

Johnson, J. M., and Satake, K. (1999), Asperity distribution of the 1952 Great Kamchatka earthquake and its relation to future earthquake potential in Kamchatka, *Pure and Applied Geophysics*, 154 (3/4), 541–553. https://link.springer.com/article/10.1007/s000240050243

MacInnes, B., Weiss, R., Bourgeois, J., and Pinegina, T K. (2010), Slip distribution of the 1952 Kamchatka Great Earthquake based on near-field tsunami deposits and historical records". *Bulletin of the Seismological Society of America*, 100 (4): 1695–1709. doi:10.1785/0120090376.

Medvedeva, A., and Rabinovich, A. (2025), Observations and numerical modelling of the Sumatra tsunami of 28 March 2005, *Journal of Marine Science and Engineering*, 13, 290. https://doi.org/ 10.3390/jmse13020290.

Miller, K. (2025), Why did such a powerful earthquake generate such a weak tsunami?". *New York Times*. 30 July 2025.

Mungov, G., Eblé, M., and Bouchard, R. (2013), DART tsunameter retrospective and real-time data: A reflection on 10 years of processing in support of tsunami research and operations, *Pure and Applied Geophysics,* 170, 1369-1384. https://doi.org/10.1007/s00024-012-0477-5.

Okada, Y. (1985), Surface deformation due to shear and tensile faults in a half-space. *Bulletin of the Seismological Society of America*, 75, 1135–1154. https://doi.org/10.1785/BSSA0750041135.

Rabinovich, A.B., and Stephenson, F.E. (2004), Longwave measurements for the coast of British Columbia and improvements to the tsunami warning capability, *Natural Hazards*, 32, (3), 313-343.

Rabinovich, A.B., Thomson, R.E., and Stephenson, F.E. (2006), The Sumatra tsunami of 26 December 2004 as observed in the North Pacific and North Atlantic oceans, *Surveys in Geophysics*, 27, 647-677.

Rabinovich, A.B., Thomson, R.E. and Fine, I.V. (2013), The 2010 Chilean tsunami off the west coast of Canada and the northwest coast of the United States, *Pure and Applied Geophysics*, 170, 1529-1565, doi 10.1007/s00024-012-0541-1.

Rabinovich, A.B., and Eblé, M. (2015), Deep-ocean measurements of tsunami waves, *Pure and Applied Geophysics*, 172(12), 3281-3312, doi: 10.1007/s00024-015-1058-1.

Rabinovich, A.B., Titov, V.V., Moore, C.W., and Eblé, M.C. (2017), The 2004 Sumatra tsunami in the southeastern Pacific Ocean: New global insight from observations and modeling, *Journal of Geophysical Research - Oceans*, 122(10), 7992-8019; doi: 10.1002/2017JC013078.

Rabinovich, A.B., Thomson, R.E., Krassovski, M.V., Stephenson, F.E., and Sinnott, D.C. (2019), Five great tsunamis of the 20th century as recorded on the coast of British Columbia, *Pure and Applied Geophysics*, 176 (7), 2887-2924; doi: 10.1007/s00024-019-02133-3.

Rabinovich, A.B., Šepić, J., and Thomson, R.E. (2023), Strength in numbers: The tail end of typhoon Songda combines with local cyclones to generate extreme sea level oscillations on the British Columbia and Washington coasts during mid-October 2016, *Journal of Physical Oceanography*, 53(1), 131-155; doi:10.1175/JPO-D-22-0096.1.

Rabinovich, A.B., Sinnott, D.C., Thomson, R.E., and Stephenson, F.E. (2025a), Estimation of resonant properties and amplification factors for Canadian Hydrographic Service tide gauge sites along the coast of British Columbia. Can. Tech. Rep. Hydrogr. Ocean Sci. 391: v + 33 p.

Rabinovich, A.B., Tsukanova, E.S., and Thomson, R.E. (2025b), The 2021 South Sandwich Islands tsunami: from the Antarctic to the far Northeast corner of the Pacific Ocea, *Geoscience Letters*, 12:56; https://doi.org/10.1186/s40562-025-00430-5

Shevchenko, G.V., Ivelskaya, T.N., and Kaistrenko, V.M. (2022), The Tsunami on November 5, 1952, in Severo-Kurilsk and its Echo in the next 70 years, *Proroda*, No.4, 1-26 [in Russian].

Soloviev S.L. (1978), Basic data on tsunamis on the Pacific coast of the USSR, Tsunami Research in the Open Ocean, Moscow, Nauka Publishing House, 61-135. (in Russian).

Steedman, E. (2025), Why Russia's megathrust earthquake was among biggest ever recorded, but damage was minimal, ABC News; https://www.abc.net.au/news/2025-07-31/

Stephenson, F.E., and Rabinovich, A.B. (2009), Tsunamis on the Pacific coast of Canada recorded in 1994-2007, *Pure and Applied Geophysics*, 166 (1/2), 177-210.

Thomson, R., Fine, I., Rabinovich, A., Mihály, S., Davis, E., Heesemann, M., and Krassovski. M. (2011), Observation of the 2009 Samoa tsunami by the NEPTUNE-Canada cabled observatory: Test data for an operational regional tsunami forecast model, *Geophysical Research Letters*, 38, L11701, doi:10.1029/2011GL046728.

Thomson R.E., and Emery, W.J. (2024), *Data Analysis Methods in Physical Oceanography*, Fourth Edition. Elsevier Science, Amsterdam, London, New York, 874 p.

Tsukanova, E., Medvedev, I., Heidarzadeh, M., and Vladimirova, I. (2025), Tsunami propagation from the 2024 Noto Peninsula earthquake across the Sea of Japan: observations and modelling, *Ocean Engineering*, 336; https://doi.org/10.1016/j.oceaneng.2025.121730

Wang, K., Thomson, R.E., Rabinovich, A.B., Fine, I.V., and Insua, T.L. (2020), The 2018 Alaska-Kodiak tsunami off the west coast of North America: A rare midplate tsunamigenic event. *Pure and Applied Geophysics*, 177(3), 1347-1378; doi.org/10.1007/s00024-019-02427-x.

Watada, S., Ksumoto, S., Satake, K. (2014), Traveltime delay and initial phase reversal of distant tsunamis coupled with the self-gravitating elastic Earth, *Journal of Geophysical Research: Solid Earth*, 119, 4287–4310, doi:10.1002/2013JB010841.

Watada, S. (2023), Progress and application of the synthesis of trans-oceanic tsunamis, *Progress in Earth and Planetary Science*, 10, 26, doi:10.1186/s40645-023-00555-1.

Weeks, S., and Studds, R.F.A. (1953), *The Tsunami of November 4, 1952 as Recorded at the Tide Gauges*. Spec. Publ. #300, U.S. Department of Commerce, Coast and Geodetic Survey, Washington, D.C., p. 62.

Zaytsev, O., Rabinovich, A.B., and Thomson, R.E. (2017), The 2011 Tohoku tsunami on the coast of Mexico: A case study. *Pure and Applied Geophysics*, 174 (8), 2961-2986; doi: 10.1007/s00024-017-1593-z.

Zaytsev, O., Tsukanova, E., Rabinovich, A.B., Thomson, R.E. (2023), The Michoacán tsunami of 19 September 2022 on the coast of Mexico: Observations, spectral properties and modelling. *Water*, 15(164). https://doi.org/10.3390/w15010164